Article

TRANSPARENT PROCESS OPEN ACCESS

THE EMBO JOURNAL

Stimulus-specific remodeling of the neuronal transcriptome through nuclear intron-retaining transcripts

Maxime Mazille, Katarzyna Buczak, Peter Scheiffele[*,†] & Oriane Mauger[**,†]

Abstract

The nuclear envelope has long been considered primarily a physical barrier separating nuclear and cytosolic contents. More recently, nuclear compartmentalization has been shown to have additional regulatory functions in controlling gene expression. A sizeable proportion of protein-coding mRNAs is more prevalent in the nucleus than in the cytosol, suggesting regulated mRNA trafficking to the cytosol, but the mechanisms underlying controlled nuclear mRNA retention remain unclear. Here, we provide a comprehensive map of the subcellular localization of mRNAs in mature mouse cortical neurons, and reveal that transcripts retained in the nucleus comprise the majority of stable intron-retaining mRNAs. Systematically probing the fate of nuclear transcripts upon neuronal stimulation, we found opposite effects on sub-populations of transcripts: while some are targeted for degradation, others complete splicing to generate fully mature mRNAs that are exported to the cytosol and mediate rapid increases in protein levels. Finally, different forms of stimulation mobilize distinct groups of intron-retaining transcripts, with this selectivity arising from the activation of specific signaling pathways. Overall, our findings uncover a cue-specific control of intron retention as a major regulator of acute remodeling of the neuronal transcriptome.

Keywords alternative splicing; immediate early gene; intron retention; neuronal activity; nuclear export

Subject Categories Neuroscience; RNA Biology

DOI 10.15252/embj.2021110192 | Received 14 November 2021 | Revised 20 August 2022 | Accepted 30 August 2022 | Published online 23 September 2022

The EMBO Journal (2022) 41: e110192

Introduction

Transcriptome remodeling plays a major role in cellular differentiation and plasticity. Modifications in RNA repertoires are highly specific to the cues received by cells. In development, regional signals and transcription factors direct transcriptomic programs that specify cell types. However, even in post-mitotic cells, transcriptomes remain dynamic to drive structural and functional changes for plasticity. In particular, mature neurons—that integrate numerous and diverse cues—have developed cue-specific pathways for transcriptome remodeling to support various forms of plasticity (Greer & Greenberg, 2008). For example, neuronal activity and growth factor signaling each trigger specific programs of *de novo* transcription resulting in the up-regulation of highly selective and specific sets of target genes that modify neuronal wiring and function (Lambert *et al*, 2013; Spiegel *et al*, 2014; Mardinly *et al*, 2016; preprint: Russek *et al*, 2019).

More recent studies revealed that subcellular compartmentalization, in particular nuclear retention of mRNAs, represents another major mechanism to control functional gene expression. In non-neuronal cells, nuclear compartmentalization plays a substantial role in transcription noise buffering which prevents stochastic mRNA fluctuations in the cytosol (Bahar Halpern *et al*, 2015; Battich *et al*, 2015). Furthermore, active nuclear retention of mRNAs is emerging as a novel form of post-transcriptional gene regulation. Notably, nuclear retention of mRNAs can be regulated through long-lasting processes such as neuronal differentiation (Yeom *et al*, 2021). Candidate gene approaches revealed that some stored nuclear transcripts can be released into the cytosol upon acute signals, thereby rapidly increasing availability of mRNAs for translation (Prasanth *et al*, 2005; Ninomiya *et al*, 2011; Boutz *et al*, 2015; Mauger *et al*, 2016; Naro *et al*, 2017). While further work is required to understand whether this is a widespread mechanism, this discovery has received considerable attention because it enhances functional gene expression independently of *de novo* transcription, a time-limiting step due to the finite processivity of the RNA polymerase II (Tennyson *et al*, 1995; Darzacq *et al*, 2007; Singh & Padgett, 2009; Fuchs *et al*, 2014; Veloso *et al*, 2014). The examination of transcript compartmentalization control is only emerging and further investigations are required to decipher its comprehensive potential in neuronal transcriptome remodeling. Notably, it remains unexplored whether this regulated mRNA compartmentalization can also selectively modify gene output upon distinct signals.

Regulated intron retention (IR) has recently emerged as one candidate mechanism for nuclear retention and signaling-induced release of mRNAs. IR is a unique form of alternative splicing and

Biozentrum of the University of Basel, Basel, Switzerland
*Corresponding author. Tel: +41 612072194; E-mail: peter.scheiffele@unibas.ch
**Corresponding author. Tel: +41 612077148; E-mail: oriane.mauger@unibas.ch
†These authors contributed equally to this work

consists of the persistence of a complete intron in otherwise mature polyadenylated mRNAs. IRs are highly prevalent and tightly regulated during development and in response to environmental signals supporting a major role in gene expression control (Jacob & Smith, 2017). IRs are a heterogeneous class of alternative splicing events that can direct their host mRNAs to multiple fates. A minority of intron-retaining transcripts (IR-transcripts) are protein coding and exported to the cytoplasm where they generate protein isoforms (Marquez *et al*, 2015; Grabski *et al*, 2021). In other cases, IR elicits the degradation of the transcript either in the nucleus or the cytoplasm (Yap *et al*, 2012; Wong *et al*, 2013; Braunschweig *et al*, 2014). More recent studies shed light on IR as a mechanism for regulating transcriptome dynamics (Ninomiya *et al*, 2011; Boutz *et al*, 2015; Mauger *et al*, 2016; Gill *et al*, 2017; Naro *et al*, 2017; Park *et al*, 2017; Pendleton *et al*, 2017, 2018). Some IR-transcripts are initially targeted for nuclear retention where they remain stored in the nucleus for many hours and several days (Mauger *et al*, 2016; Naro *et al*, 2017). These transcripts form a reservoir of RNAs that can be released into the cytosol upon signals through splicing completion independently of new transcription. Interestingly, intron retention programs appear to target different sets of transcripts in different cellular systems. In neurons, an elevation of network activity and calcium influx has been shown to rapidly lead to the splicing completion of transcripts encoding proteins involved in cytoskeletal regulation and signaling pathways (Mauger *et al*, 2016). By contrast, in male gametes, some mRNAs coding for proteins implicated in spermatogenesis are subject to splicing completion in the latest stage of gametogenesis (Naro *et al*, 2017). The difference in the identity of regulated transcripts likely reflects cell class-specific IR programs. However, it remains unexplored whether stimuli trigger splicing completion of IR-transcripts by releasing a common brake of intron excision or whether there are cue-specific IR programs controlled through dedicated signaling pathways. Noteworthy, in yeast, different cellular stresses modify the splicing kinetics of distinct sets of constitutively spliced introns (Bergkessel *et al*, 2011). Moreover, multiple signaling pathways have been implicated in the regulation of alternative exon choices in response to external stimuli (Matter *et al*, 2002; Shin & Manley, 2004; Zhou *et al*, 2012). This raises the possibility that distinct cues and signaling may target select IR programs in other systems including mature neurons.

In the present study, we systemically mapped the subcellular localization of neuronal IR-transcripts and their response to neuronal stimuli. We found that the majority of transcripts that stably retain introns are subject to nuclear retention. After neuronal stimulation, the vast majority of transcripts that complete splicing are exported to the cytosol and translated indicating that IR is a widespread mechanism to control storage and on-demand release of mRNAs from the nucleus for functional gene expression. Remarkably, stimulation with brain-derived neurotrophic factor versus a brief elevation of neuronal network activity mobilizes distinct pools of IR-transcripts. This cue-specificity of IR programs arises from the engagement of distinct signaling pathways that convey specific messages to the neuronal nucleus. Overall, we conclude that IR programs allow a rapid, transcription-independent and cue-specific remodeling of neuronal transcriptome during plasticity.

Results

The majority of stable intron-retaining transcripts are localized in the nucleus

To systematically assess sub-cellular localization of transcripts with stable intron retentions (IR), we developed a dedicated experimental workflow. We performed biochemical cell fractionation (Suzuki *et al*, 2010) and separated nuclear and cytosolic RNAs of mature mouse primary neocortical cells (Fig 1A). To solely analyze the population of stable intron-retaining transcripts (IR-transcripts) rather than transcripts containing transient IRs, we pharmacologically blocked transcription for 3 h before collecting cells (Fig EV1A). For each sample, whole-cell extract, nuclear-enriched (designated as "Nucleus") and cytosolic-enriched (designated as "Cytosol") compartments, polyadenylated (poly(A)+) RNAs were isolated from three biological replicates and spike-in RNAs were added to assess the absolute nuclear-to-cytosol ratio of expressed transcripts (see Materials and Methods). Samples were sequenced at high depth (ca. 100 million reads per sample, 100-mer reads). Ribosomal RNAs

Figure 1. The majority of stable intron-retaining transcripts are localized in the nucleus.

A Quality of the cell fractionation assays was controlled by western blot by assessing the distribution of nuclear and cytosolic markers in the whole cell extract (WCE), the cytosol and the nucleus. Protein lysates were isolated from mouse primary neocortical cells (14 days in culture) treated for 3 h with the transcription inhibitor triptolide (1 μM) (four independent cultures).

B Top: percentage of intron retention (PIR) is assessed as the ratio between the IR-transcript expression and the total transcript expression (sum of intron-retaining and spliced transcripts). Introns are considered retained if minPIR ≥ 20 in WCE (see Materials and Methods); 1,465 IRs were then identified. Bottom: Violin plot displaying the PIR distribution in the whole cell extract (WCE, black), cytosol (blue) and nucleus (green) of i) all introns (left) and ii) the 1,465 retained introns (right). For the inner boxplot, the central line represents the median; the upper and lower bounds of the box represent, respectively, the 75th (Q3) and 25th (Q1) percentiles; the upper whisker corresponds to the highest observed value within [Q3, 1.5*Q3] and the lower whisker corresponds to the lowest observed value within [0.5*Q1, Q1] (three independent cultures).

C Pairwise comparison of the expression of the 1,465 intron-retaining isoforms (IR) in nuclear versus cytosolic fractions. IR-transcripts enriched in the nucleus are labeled in green (nuclear-to-cytosol expression ratio ≥ 2); IR-transcripts enriched in the cytosol are labeled in blue (nuclear-to-cytosol expression ratio ≤ 0.5).

D Violin plots displaying the nucleus-to-cytosol expression ratio of the 1,465 intron-retaining isoforms (left, N = 1,465) and all expressed spliced transcripts (right, N = 118,436). Percentage of nuclear-enriched (green) and cytosolic-enriched (blue) transcripts are indicated on the panel. For the inner boxplot, the central line represents the median; the upper and lower bounds of the box represent, respectively, the 75th (Q3) and 25th (Q1) percentiles; the upper whisker corresponds to the highest observed value within [Q3, 1.5*Q3] and the lower whisker corresponds to the lowest observed value within [0.5*Q1, Q1].

E–H Violin plots displaying 5′ splice-site strength (E), 3′ splice-site strength (F), intron length (G) and GC content (H) of canonically spliced introns (gray, N = 116,971), nuclear IRs (green, N = 820) and cytosolic IRs (blue, N = 274). The central dots represent the median. The P-values calculated with a two-tailed Mann–Whitney test are indicated on the top of each panel.

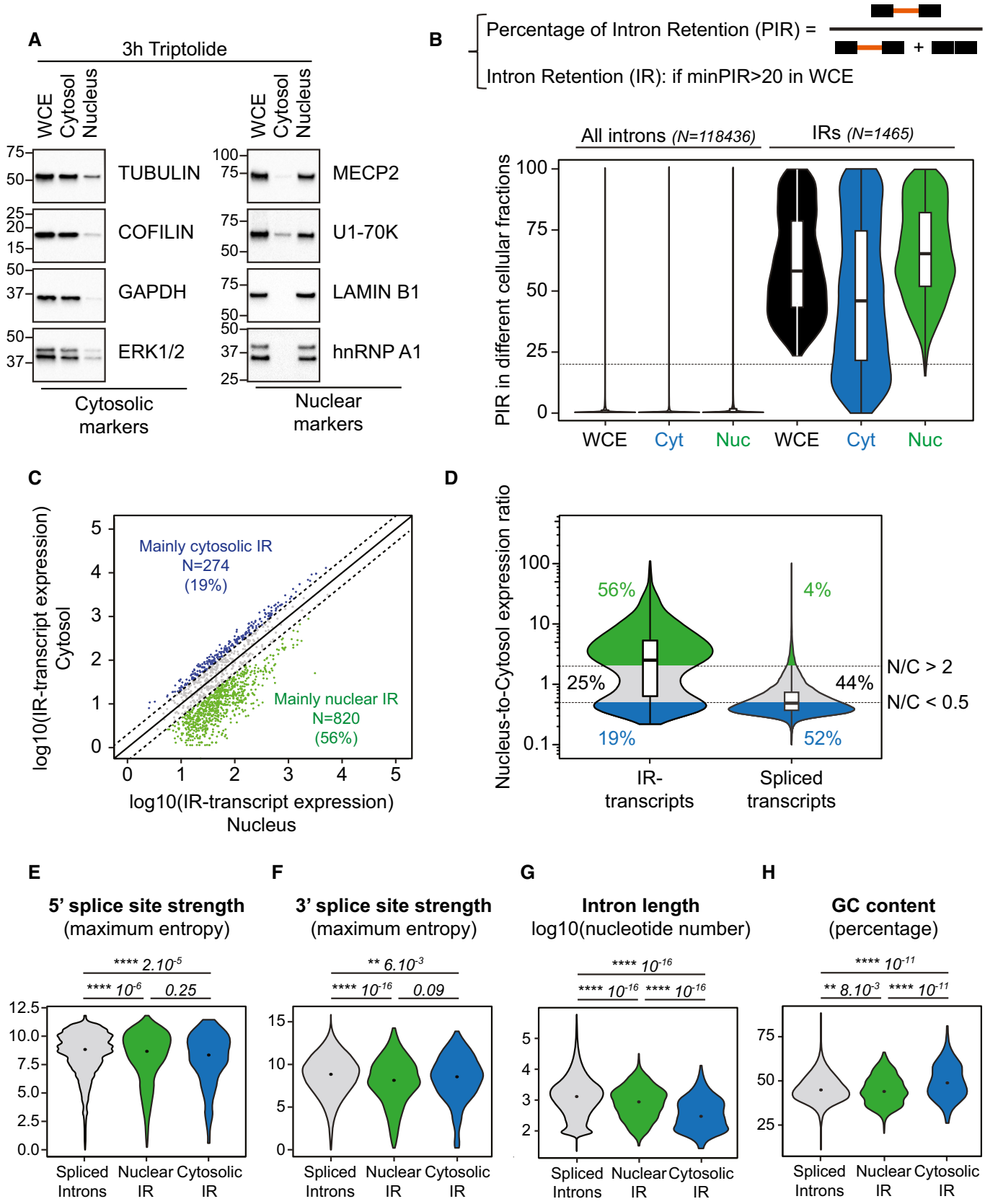
A
3h Triptolide
WCE
Cytosol
Nucleus
TUBULIN
COFILIN
GAPDH
ERK1/2
MECP2
U1-70K
LAMIN B1
hnRNP A1
Cytosolic markers
Nuclear markers
B
Percentage of Intron Retention (PIR) =
Intron Retention (IR): if minPIR>20 in WCE
All introns (N=118436)
IRs (N=1465)
PIR in different cellular fractions
WCE
Cyt
Nuc
C
Mainly cytosolic IR
N=274
(19%)
Mainly nuclear IR
N=820
(56%)
log10(IR-transcript expression) Cytosol
log10(IR-transcript expression) Nucleus
D
Nucleus-to-Cytosol expression ratio
56%
4%
25%
44%
19%
52%
N/C > 2
N/C < 0.5
IR-transcripts
Spliced transcripts
E
5' splice site strength
(maximum entropy)
**** 2.10-5
**** 10-6
0.25
Spliced Introns
Nuclear IR
Cytosolic IR
F
3' splice site strength
(maximum entropy)
** 6.10-3
**** 10-16
0.09
G
Intron length
log10(nucleotide number)
**** 10-16
H
GC content
(percentage)
**** 10-11
** 8.10-3

Figure 1.

represented ca. 1% of the mapped reads (Table 1), indicating that the enrichment of poly(A) + RNAs was highly efficient.

For every intron of the mouse genome, we analyzed the percentage of intron retention (PIR) with a validated computational pipeline (Mauger *et al*, 2016; see Materials and Methods, Appendix Fig S1 and Table S1; Figs 1B and EV1B). Introns were considered as retained if the PIR value was higher than 20 in whole cell extract. Similar to a previous analysis (Mauger *et al*, 2016), we identified 1,465 stable IRs arising from 922 genes—among 11,381 genes expressed in primary neocortical neurons (Fig EV1C; Dataset EV1). The vast majority of genes with stable IR exhibited only 1 or 2 retention events (Fig EV1D). We then probed the distribution of intron retention levels for these events in each subcellular compartment (Fig 1B). We found that PIR values were overall higher in the "Nucleus" than in the "Cytosol" (mean $PIR_{Nucleus} = 66$; mean $PIR_{Cytosol} = 48$) suggesting that stable IR-transcripts are

Table 1. Summary of RNA sequencing read alignment.

		Total Reads	Uniquely mapped reads	Mapped to too many loci	Mapped to multiple loci	Unmapped reads: too short	Unmapped reads: other	RIBOSOMAL	CODING	UTR	INTRONIC	INTERGENIC	mRNA
Pooled samples during sequencing	Cytosol_ Ctl_Rep1	102,381,005	**87.31%**	0.19%	7.40%	5.04%	0.07%	**0.9%**	41.0%	37.2%	3.3%	17.8%	78.1%
	Cytosol_ Ctl_Rep2	99,258,948	**87.81%**	0.19%	7.25%	4.68%	0.07%	**0.8%**	43.6%	35.4%	3.1%	17.1%	79.0%
	Cytosol_ Ctl_Rep3	101,852,925	**86.03%**	0.17%	8.02%	5.71%	0.07%	**0.8%**	41.4%	35.4%	3.1%	19.4%	76.8%
	Nucleus_ Ctl_Rep1	92,173,824	**87.25%**	0.28%	6.69%	5.53%	0.25%	**1.5%**	35.4%	32.6%	10.3%	20.3%	68.0%
	Nucleus_ Ctl_Rep2	96,510,469	**87.87%**	0.26%	6.41%	5.23%	0.23%	**1.5%**	37.7%	31.9%	9.7%	19.2%	69.6%
	Nucleus_ Ctl_Rep3	94,707,116	**86.22%**	0.26%	7.04%	6.25%	0.23%	**1.1%**	36.9%	31.5%	9.9%	20.6%	68.4%
	WCE_ Ctl_Rep1	108,853,793	**87.62%**	0.22%	6.89%	5.14%	0.14%	**1.3%**	39.8%	34.7%	6.1%	18.2%	74.5%
	WCE_ Ctl_Rep2	100,207,337	**87.11%**	0.23%	6.60%	5.90%	0.15%	**1.1%**	41.6%	33.2%	6.6%	17.6%	74.8%
	WCE_ Ctl_Rep3	95,864,215	**86.70%**	0.21%	7.61%	5.32%	0.15%	**1.1%**	38.9%	33.3%	6.6%	20.1%	72.2%
	Cytosol_ Bic_Rep1	88,611,820	**87.28%**	0.20%	7.07%	5.37%	0.08%	**0.8%**	42.4%	36.2%	3.5%	17.1%	78.6%
	Cytosol_ Bic_Rep2	105,010,780	**87.69%**	0.20%	6.96%	5.08%	0.07%	**0.8%**	44.8%	34.8%	3.1%	16.5%	79.6%
	Cytosol_ Bic_Rep3	96,224,784	**87.79%**	0.19%	6.95%	4.99%	0.08%	**0.7%**	43.6%	35.8%	3.2%	16.8%	79.4%
	Nucleus_ Bic_Rep1	103,873,601	**88.72%**	0.26%	6.17%	4.64%	0.21%	**1.1%**	37.8%	34.6%	8.3%	18.2%	72.5%
	Nucleus_ Bic_Rep2	91,452,042	**87.14%**	0.27%	5.92%	6.44%	0.24%	**1.2%**	38.5%	32.1%	9.9%	18.4%	70.5%
	Nucleus_ Bic_Rep3	104,217,750	**87.36%**	0.24%	6.79%	5.41%	0.19%	**1.0%**	39.5%	32.3%	8.0%	19.3%	71.8%
	WCE_ Bic_Rep1	99,460,363	**87.90%**	0.23%	6.37%	5.37%	0.14%	**1.0%**	41.0%	35.3%	5.8%	16.9%	76.3%
	WCE_ Bic_Rep2	108,118,242	**87.77%**	0.23%	6.44%	5.43%	0.14%	**1.1%**	43.0%	33.4%	5.7%	16.8%	76.5%
	WCE_ Bic_Rep3	85,634,802	**87.53%**	0.22%	6.87%	5.27%	0.12%	**0.9%**	42.9%	33.8%	5.1%	17.4%	76.6%
Pooled samples during sequencing	Ctl_Rep1	120,787,493	**88.77%**	0.25%	6.30%	4.60%	0.09%	**0.9%**	48.5%	31.7%	5.0%	13.9%	80.2%
	Ctl_Rep2	115,636,180	**89.20%**	0.23%	6.18%	4.29%	0.10%	**0.7%**	47.2%	31.8%	6.2%	14.1%	79.0%
	Ctl_Rep3	121,220,186	**88.04%**	0.23%	6.71%	4.92%	0.09%	**0.7%**	46.1%	32.8%	5.6%	14.9%	78.9%
	Bic_Rep1	133,680,600	**88.60%**	0.24%	6.65%	4.43%	0.09%	**0.9%**	47.4%	32.4%	4.7%	14.6%	79.7%
	Bic_Rep2	106,630,731	**89.55%**	0.23%	5.84%	4.26%	0.12%	**0.6%**	47.1%	31.4%	7.2%	13.8%	78.5%
	Bic_Rep3	168,099,149	**87.95%**	0.25%	7.17%	4.55%	0.09%	**0.8%**	45.9%	33.4%	4.6%	15.4%	79.3%
	BDNF_Rep1	108,996,997	**88.77%**	0.25%	6.28%	4.61%	0.09%	**1.0%**	48.6%	31.6%	5.0%	13.9%	80.2%
	BDNF_Rep2	186,854,844	**89.56%**	0.26%	5.81%	4.28%	0.10%	**0.6%**	48.2%	31.7%	6.3%	13.2%	79.9%
	BDNF_Rep3	142,143,812	**88.69%**	0.25%	6.23%	4.71%	0.11%	**0.7%**	47.5%	31.4%	6.3%	14.0%	79.0%

Uniquely mapped reads were used for the read normalisation of each sample (in bold). The low proportion of ribosomal reads was used as an indirect readout of the high efficiency of polyA RNA enrichment (in bold).

predominantly localized to the nucleus. To confirm this, we compared the expression of intron-retaining isoforms in the "Nucleus" and "Cytosol" samples (Fig 1C and D). We calculated an absolute nuclear-to-cytosol ratio using the spike-in RNAs for normalizing nuclear and cytosolic reads (see Materials and Methods). Among the 1,465 IR-transcript isoforms, 820 (56%) were strongly enriched in the "Nucleus" (nucleus-to-cytosol ratio > 2), while 274 (19%) were more abundant in the "Cytosol" (nucleus-to-cytosol ratio < 0.5); the remaining isoforms (25%) were similarly detected in the "Nuclear" and the "Cytosolic" fractions. By contrast, only a minority of fully spliced transcripts is enriched in the "Nucleus" (4%) and the majority of them is highly enriched in the "Cytoplasm" (52%). This indicates that the prevalence of IR-transcripts in the "Nucleus" samples is not a consequence of an inefficient biochemical fractionation (Fig 1D).

Thus, our data reveal an unprecedented large population of stable IR-transcripts predominantly localized in the nucleus and suggest that IR could represent a general mechanism for nuclear compartmentalization of mRNAs in neurons.

Stable nuclear IRs share features with canonical spliced introns

We hypothesize that the nuclear localization of stable IR-transcripts is intronically encoded. To test this hypothesis, we examined whether the nuclear IRs harbor specific sequence properties. Nuclear-retained introns exhibit weak 5′ and 3′ splice sites compared to canonically spliced introns—a general property of IRs (Braunschweig *et al*, 2014; Boutz *et al*, 2015; Mauger *et al*, 2016; Ullrich & Guigó, 2020; Yeom *et al*, 2021). However, the splice-site strength of stable nuclear retained introns is indistinguishable from the one of cytosolic-retained introns (Fig 1E and F). Thus, the splice-site sequences themselves are not dictating the nuclear localization of IR-transcripts.

However, stable nuclear-retained introns display specific features in terms of length and GC content; while nuclear-retained introns remain shorter than spliced introns, they are markedly longer than cytosolic-retained introns (Fig 1G). Similarly, GC content of nuclear retained introns is lower than the one of cytosolic retained introns and comparable to GC content of canonical spliced introns (Fig 1H).

To conclude, in respect to several sequence features, stable nuclear IRs resemble canonically spliced introns and retention can be regulated by trans-acting factors. Thus, we hypothesize that a substantial proportion of stable nuclear-retained introns preserves the ability to be excised through splicing; but as opposed to canonical spliced introns, enhancing cues may be required to promote their removal.

Nuclear intron-retaining transcripts are regulated by several forms of neuronal stimulation

Intron retention rates have been reported to be regulated over days of neuronal differentiation (Yap *et al*, 2012; Braunschweig *et al*, 2014; Yeom *et al*, 2021) or in mature neurons in response to acute elevation of neuronal network activity (Mauger *et al*, 2016). Mature neurons exhibit specific forms of plasticity in response to specific plasticity cues. To explore whether such cues can acutely target subsets of IRs for rapid transcriptome remodeling, we first probed whether different stimuli can regulate IRs in mature neocortical neurons. We used two modes of neuronal stimulation. On the one hand, mouse primary neocortical cultures were treated for 1 h with bicuculline, an antagonist of $GABA_A$ receptors. Bicuculline-dependent blockade of GABAergic transmission results in robust increase in neuronal network activity. On the other hand, mouse primary neocortical cultures were treated for 1 h with the brain-derived neurotropic factor (BDNF) which is specifically released during forms of synaptic plasticity and facilitates long-term potentiation (Gottmann *et al*, 2009; Harward *et al*, 2016). In either condition, cells were treated with a transcription inhibitor to solely focus on IR-transcripts that are stable in unstimulated neocortical cells (Fig EV2A). Given that this study exclusively focuses on such stable IR-transcripts, we will simply designate them as "IR-transcripts" in the remainder of the manuscript. Bicuculline and BDNF robustly activate intracellular signaling pathways (Fig EV2B). Notably, both, bicuculline and BDNF stimulation induced a robust increase of ERK phosphorylation in nearly all neurons, indicating that both treatments stimulated the vast majority of neurons in culture (Figs 2A and B, and EV2C and D). Interestingly, we found that both bicuculline and BDNF stimulation regulate a sizeable set of IR-transcripts in the absence of *de novo* transcription. Upon bicuculline treatment, the expression level of 430 IR-transcripts was altered (fold-change > 20% and |z-score| > 1.5); 382 IR-transcripts exhibit a lower expression upon stimulation (resulting from induced splicing or degradation, see Fig 3) and 48 transcripts were up-regulated (resulting from inhibition of basal splicing or enhanced stabilization, see Fig 3) (Figs 2C and EV2E; Datasets EV2 and EV3). BDNF stimulation modified the expression of 385 IR-transcripts (243

Figure 2. Nuclear intron-retaining transcripts are regulated by several forms of neuronal stimulation.

A, B Efficiencies of bicuculline (A) and BDNF (B) stimulation were assessed by controlling the induction of ERK phosphorylation by immunostaining. Mouse primary neocortical cells (14 days in culture) were stimulated with bicuculline (20 μM) to elevate the neuronal network excitation or with the brain-derived neurotrophic factor BDNF (50 ng/ml) for 5 min. Cells were stained with anti-phospho-ERK (green, bottom) and anti-MAP2 (white, top) antibodies and counterstained with Hoechst (blue, top) (four independent cultures).

C, D Volcano plots displaying the expression fold change (FC) of IR-transcripts and the corresponding z-score (absolute value) upon bicuculline (C) and BDNF (D) stimulation. DRB (50 μM) was applied to mouse primary neocortical cells for 2 h; 1 h before cell collection, bicuculline (20 μM) or BDNF (50 ng/ml) were applied or not (control). Every transcript retaining an intron (minPIR ≥ 20%) in unstimulated condition is plotted. IR-transcripts were considered down-regulated (light blue or orange) or up-regulated (dark blue or red) if the followings are applied: fold change of IR-transcript expression ≥ 20% and |z-score| ≥ 1.5 (three independent cultures).

E, F Pairwise comparison of the expression of regulated IR-transcripts in the nuclear and the cytosolic fractions of unstimulated mouse primary neocortical cells. Every transcript retaining an intron (minPIR ≥ 20%) in whole cell extract is plotted. Intron-retaining transcripts down- or up-regulated upon bicuculline stimulation (E) are labeled in light blue and dark blue, respectively, and those down- or up-regulated upon BDNF stimulation (F) are labeled in orange and red, respectively (three independent cultures).

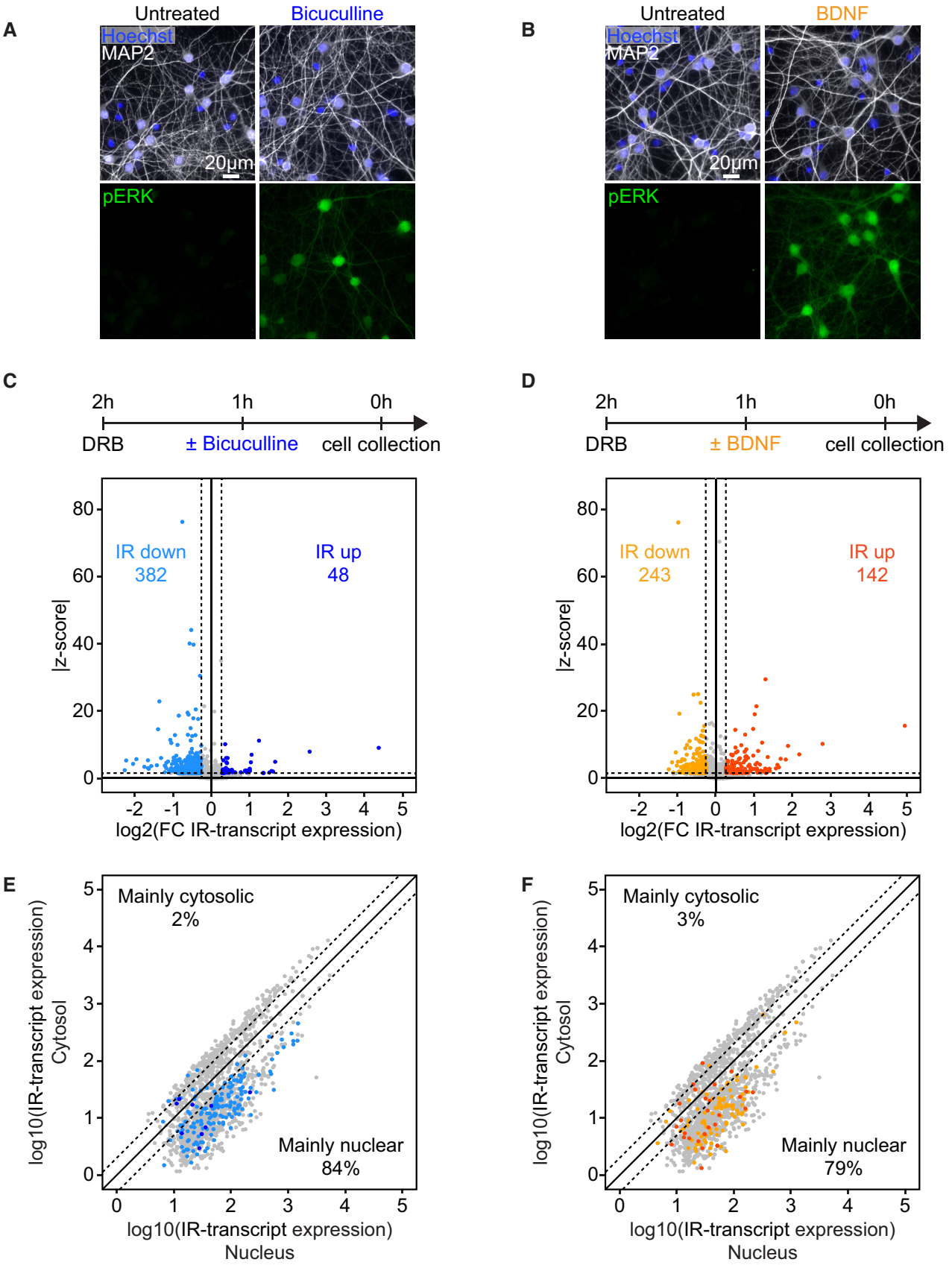

Figure 2.

down-regulated and 142 up-regulated) (Figs 2D and EV2E; Datasets EV2 and EV3). Individual regulated introns were observed all along 5′-3′ extent the transcripts (Fig EV2F). Importantly, on average, regulated IR-transcripts are expressed at a similar level as unregulated IR-transcripts (Fig EV2G). Thus, these mRNAs constitute a major transcript pool rather than a lowly expressed subpopulation. The vast majority of regulated IR-transcripts were localized in the nucleus (nucleus-to-cytosol ratio > 2; 84 and 79% of bicuculline- and BDNF-sensitive IR-transcripts, respectively) (Fig 2E and F). Remarkably, the population of regulated transcripts is even more enriched in the nucleus than the overall population of IR-transcripts (two-tailed Mann–Whitney test, P-value < 10^{-5} for both bicuculline- and BDNF-regulated transcripts) (Fig EV2H).

Thus, our data reveal that multiple plasticity cues target nuclear IR-transcripts. We hypothesize that a large population of IRs can be regulated through nuclear processes including splicing.

Neuronal stimulation regulates intron-retaining transcripts through splicing and degradation processes

The fate of IR-transcripts and their contribution to protein production is determined by the rates of splicing, degradation, and nuclear export. Each of these processes could be targeted for establishing specific transcriptome modifications in response to distinct forms of neuronal stimulation. Hence, before thoroughly probing the cue-specificity of IR programs, we dissected the contribution of degradation and splicing for the two forms of neuronal stimulation. We performed a pairwise comparison of the expression regulation of IR-transcripts and their counterpart spliced transcripts. Upon splicing, the decrease of intron-retaining isoforms is accompanied by an increase of the spliced isoforms. Applying stringent criteria to select IRs that follow this scheme (see Materials and Methods), we found that 83 and 46 IR-transcripts underwent splicing completion upon neuronal stimulation with bicuculline and BDNF, respectively (Figs 3A and B, and EV3A and B; Datasets EV2 and EV3). We performed targeted validations using semi-quantitative PCR and real-time quantitative PCR assays for several IR-transcripts. Notably, the transcripts encoding the AMPA receptor subunit GRIA3 and the transcription factor TCF25 exhibit a concomitant decrease of the intron-retaining isoforms and an increase of the spliced isoforms confirming their regulation through splicing induction (Figs 3C and EV3C). We further validated a decrease of the intron-retaining isoforms and concomitant increase of the spliced isoforms of transcripts encoding the cytoskeletal regulator FNBP4 and the transcript arising from the microRNA containing gene Mirg (Figs 3D and EV3D). Interestingly, we also identified IR-transcripts that showed increased retention and reduced levels of the spliced isoforms upon neuronal stimulation (2 for bicuculline, 7 for BDNF). This indicates that intron excision can also be slowed-down in response to signaling. Note that the apparent low number of IR-transcripts that undergo reduced splicing results from the fact we focused our analysis on IR-transcripts that were stable before stimulation; that is, those associated with IRs whose retention level remains higher than 20% after transcription inhibition.

Remarkably, our data also reveal that a substantial population of regulated IRs cannot readily be explained by a splicing mechanism. Many IRs were associated with spliced and intron-retaining isoforms regulated in the same direction. They were either both increased or decreased suggesting a respective overall stabilization or degradation not instructed by IRs (Fig 3A and B). We also found a sizeable set of regulated IR-transcripts whose spliced counterpart was not regulated (see Materials and Methods) suggesting that induced degradation/stabilization process was specifically targeting the IR-transcript isoforms (Figs 3A and B, and EV3A and B). Note that in some cases, these events could also arise from a splicing reaction targeting other splice sites; however, our pipelines did not detect examples for such cases. Notably, 46 and 29 transcripts were destabilized upon stimulation with bicuculline and BDNF, respectively. Interestingly, while our analysis focused on IR-transcripts that were stable in unstimulated conditions, we also found that a few (4 and 13) IR-transcripts were even more stable upon neuronal stimulation with bicuculline or BDNF. PCR assays confirmed the reliable identification of such regulation by degradation. For example, the transcript encoding the DNA double strand regulator CCDC136 exhibits a consistent decrease of intron-retaining isoforms but no change in the spliced isoforms in response to bicuculline stimulation (Figs 3E and EV3C). Similar regulation was observed for the transcripts encoding the brain-specific actin regulator KLHL17 upon BDNF application (Figs 3F and EV3D).

In aggregate, our data support that in mature neocortical neurons, neuronal signaling not only drives transcription-independent modifications of the neuronal transcriptome through splicing completion but also through transcript-specific degradation.

Figure 3. Neuronal stimulation regulates intron-retaining transcripts through splicing and degradation processes.

A, B Pairwise comparison of the expression fold change (FC) of intron-retaining isoforms (IR) and the spliced isoforms upon bicuculline (A) or BDNF (B) stimulation. In all conditions, DRB (50 μM) was applied to mouse primary neocortical cells (14 days in culture) for 2 h; 1 h before cell collection, bicuculline (20 μM) or BDNF (50 ng/ml) were applied or not (control). Every transcript containing a retained intron (minPIR > 20) in control condition is plotted. IR-transcripts that are considered regulated through splicing if the followings are applied: (i) IR-isoform expression fold change ≥ 20% and |z-score| ≥ 1.5, (ii) spliced isoform expression fold change ≥ 20% and |z-score| ≥ 1.5 and (iii) expression of the IR-isoforms and the spliced isoforms evolved in opposite directions. IR-transcripts that are considered regulated through degradation (IR-transcript specific decrease) if the followings are applied: (i) IR expression fold change ≥ 20% and |z-score| ≥ 1.5 and (ii) spliced expression fold change ≤ 5% and |z-score| ≤ 1 (three independent cultures).

C–F RT-PCR validations of regulated IR-transcripts through splicing upon bicuculline stimulation (C) and BDNF stimulation (D) and through degradation upon bicuculline stimulation (E) and BDNF stimulation (F). Expression of the IR-isoforms and the spliced isoforms were analyzed by semi-quantitative PCR (left panels). Means and SDs (standard deviations) of PIR values are shown beneath each panel. In addition, fold changes in the expression of the IR-transcripts (red and orange) and spliced (dark gray) isoforms were assessed with real-time qPCR using three different primer sets, as represented in the top scheme. Means and SDs are displayed (3–4 independent cultures); the P-values calculated with a one-tailed paired t-test are indicated (as numerical values when $P > 0.05$, as * when $P < 0.05$, as ** when $P < 0.01$ and as *** when $P < 0.001$). Note that the Gria3 spliced transcript (C) does not correspond to the canonical mRNAs and presumably arise from a first step of recursive splicing and thereby likely require splicing completion to generate fully mature Gria3 transcripts (Sibley *et al*, 2015).

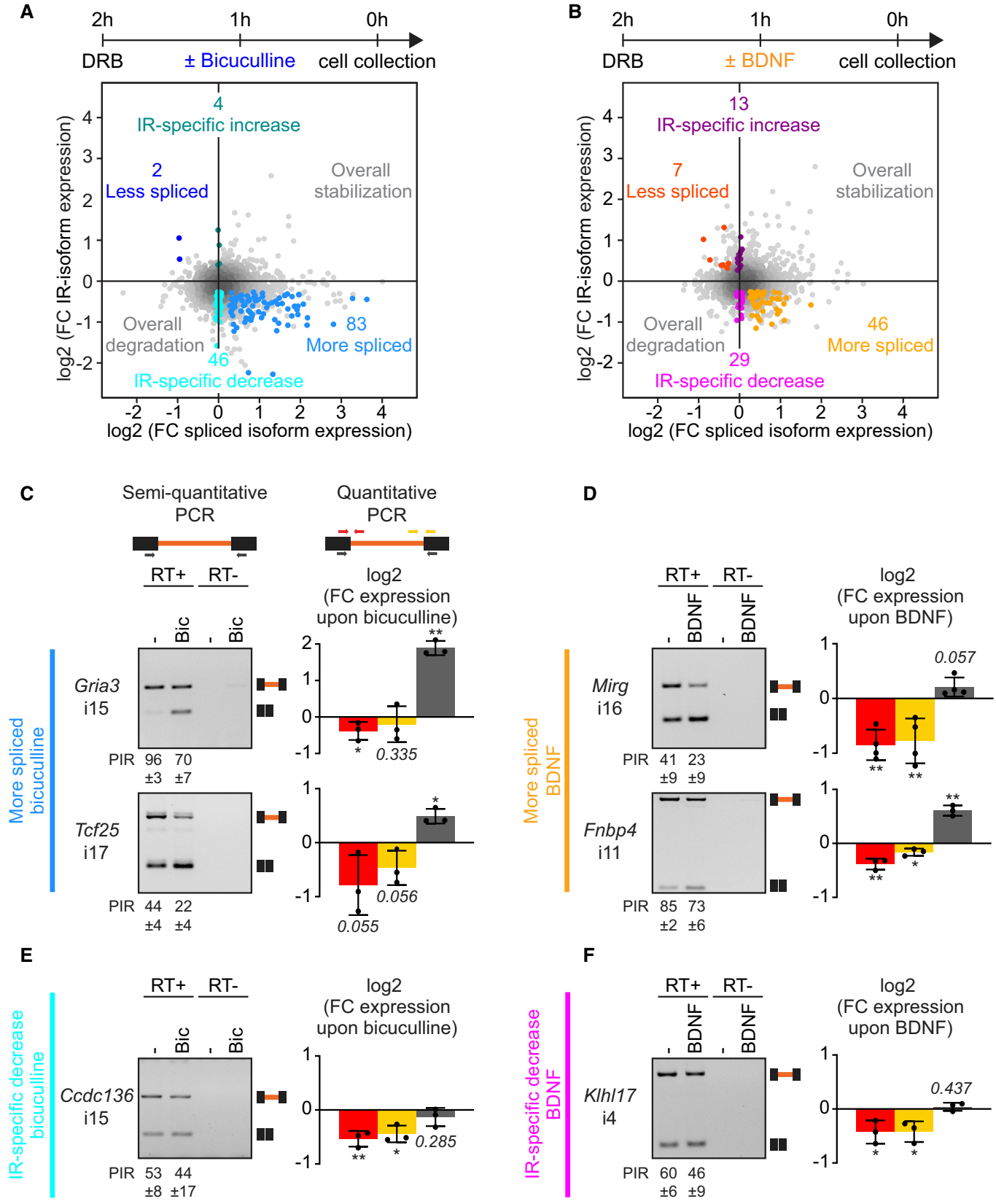

Figure 3.

Activity-dependent splicing of intron-retaining transcripts is associated with increased cytosolic mRNAs and protein synthesis

To test whether neuronal activity-dependent splicing completion is followed by nuclear export and translation, we systematically probed the localization of IR-transcripts and their spliced mRNA counterparts in the nucleus and the cytosol 1 h after bicuculline-mediated elevation of neuronal network activity. First, we mapped the total cellular repertoire of IRs and regulated IR-transcripts (based on whole cell extract samples, same criteria than in previous figures, see Materials and Methods). Nearly, all regulated IR-transcripts were predominantly localized to the nucleus (Fig EV4A). As expected, IR-transcripts regulated through splicing (based on whole cell extract data) were significantly less abundant in the nucleus in response to bicuculline stimulation (consistent with splicing being a nuclear process) (Figs 4A and B, EV4B; Dataset EV1). A concomitant increase of the spliced isoforms was also observed in the nucleus upon stimulation (Fig 4A and B). Remarkably, we found that the spliced transcripts were also significantly enriched in the cytosol 1 h after bicuculline application supporting the newly spliced transcripts were exported to the cytosol after splicing completion (Figs 4A and B, and EV4B). By contrast, unregulated IR-transcripts and the corresponding spliced isoforms were almost unchanged upon stimulation in both nuclear and cytosolic compartments (Fig EV4C).

These data support that after splicing completion, the newly spliced transcripts isoforms are exported to the cytosol making them available for translation. We then tested whether these mRNAs are indeed used for protein synthesis. To address this point, using a PRM (Parallel Reaction Monitoring) mass spectrometry approach, we analyzed the protein levels of several genes containing a regulated retained intron. Remarkably, we found a significant increase in the protein levels of most tested candidates (7 on 9) 2 h after bicuculline stimulation (Fig 4C). For instance, RIMBP2—a component of the presynaptic active zone, DDHD2—an actor of membrane trafficking—and the kinases CLK1 and CLK4 are up-regulated in response to bicuculline stimulation. Noteworthy, the protein increase occurred independently of transcription. This suggests that protein elevation arises from the translation of newly spliced transcripts generated through activity-dependent intron excision.

In sum, our data support the hypothesis that IR enables the nuclear compartmentalization of transcripts and their removal through splicing completion represents a widely used mechanism for stimulus-dependent release of transcripts into the cytosol, thereby rapidly making them available for translation. Importantly, this major form of gene regulation occurs in the absence of alterations in total transcript levels (Fig EV4D) and, thus, is not detectable with conventional transcriptomic methods.

Stimulus-specific regulation of sub-populations of intron retentions

Neurons undergo distinct forms of plasticity in response to specific cues. Thus, we wondered whether the regulation of IR programs exhibits cue-specific mobilization of specific transcript pools. We compared the regulation of IR-transcripts upon stimulation with bicuculline and BDNF (Fig 5A and B; Datasets EV2 and EV3). This analysis clearly revealed three major categories of IR-transcripts: (i) IR-transcripts that are regulated by both bicuculline and BDNF stimulation, (ii) IR-transcripts that are solely regulated by bicuculline stimulation, and (iii) IR-transcripts only affected by BDNF stimulation.

For the category of commonly regulated IR-transcripts, 113 and 29 IR-transcripts were respectively down- and up-regulated by both bicuculline and BDNF stimulation (Fig 5B). For instance, the transcript encoding the metabolic enzyme NDST3 associated with schizophrenia is regulated upon both bicuculline and BDNF stimulation (Figs 5C and EV5A and B). Nevertheless, *Ndst3* regulation harbors specificity as another stimulus (the group I metabotropic glutamate receptor agonist DHPG) did not impact its IR profile (Fig 5C). Among commonly regulated transcripts, we could identify 12 high confidence IR-transcripts regulated by splicing and 4 transcripts regulated by degradation (Dataset EV3). Note that because we used very stringent criteria to identify transcripts regulated through splicing versus degradation, we could not confidently assign many of regulated IR-transcripts—identified in Fig 3—to splicing or degradation.

Remarkably, a sizeable population of IR-transcripts were specifically regulated by only one mode of stimulation (Fig 5A and B). Using stringent criteria (fold-change < 5% for unregulated events, see Materials and Methods), we confidently identified 48 and 34 IR-transcripts solely regulated upon bicuculline or BDNF stimulation, respectively. For example, the IR-transcripts encoding the AMPA receptor subunit GRIA3 and the transcription factor TCF25 are only regulated upon bicuculline stimulation but do not exhibit any change in response to BDNF application (Fig 5D and EV5A and B). To further probe the selective regulation of these targets, we used the group I mGluR agonist DHPG and similarly found no change in IR in these transcripts (Fig 5D). By contrast, the transcripts arising from the miRNA-containing gene Mirg and the transcripts encoding the brain-specific actin regulator KLHL17 are exclusively regulated by BDNF stimulation but not upon stimulation with bicuculline or DHPG (Figs 5E and EV5A and B).

Another striking category of specific IRs is associated with IR-transcripts that are bi-directionally regulated upon bicuculline versus BDNF stimulation. More precisely, some cue-specific IR-transcripts are regulated upon both bicuculline and BDNF stimulation but in opposite directions (Fig 5B). For instance, the IR-transcripts encoding the splicing factor SRSF2 undergo degradation upon stimulation with bicuculline, while BDNF signaling stabilized them (Figs 5F and EV5B).

In sum, our data reveal that regulated IR-transcripts can be subdivided in several classes: some IRs are commonly regulated by bicuculline and BDNF stimulation, whereas others are cue-specific. Thus, targeting IRs represents a way to specifically remodel the neuronal transcriptome upon distinct forms of neuronal stimulation.

Stimulation-specificity of intron retention programs is conveyed by distinct signaling pathways

To obtain insight into the mechanism of neuronal cue-specific regulation of IR, we probed the signaling pathways involved in stimulated intron excision. Neuronal activity-dependent signaling elicited by elevation of network activity by bicuculline treatment relies on calcium signaling either through NMDA receptors or voltage-dependent calcium channels. As for BNDF-signaling events, they largely depend on the mitogen-activated protein kinase (MAPK) pathway. We thus wondered whether the stimulation-specificity of IR programs is conveyed by the differential activation of calcium signaling and MAPK pathways.

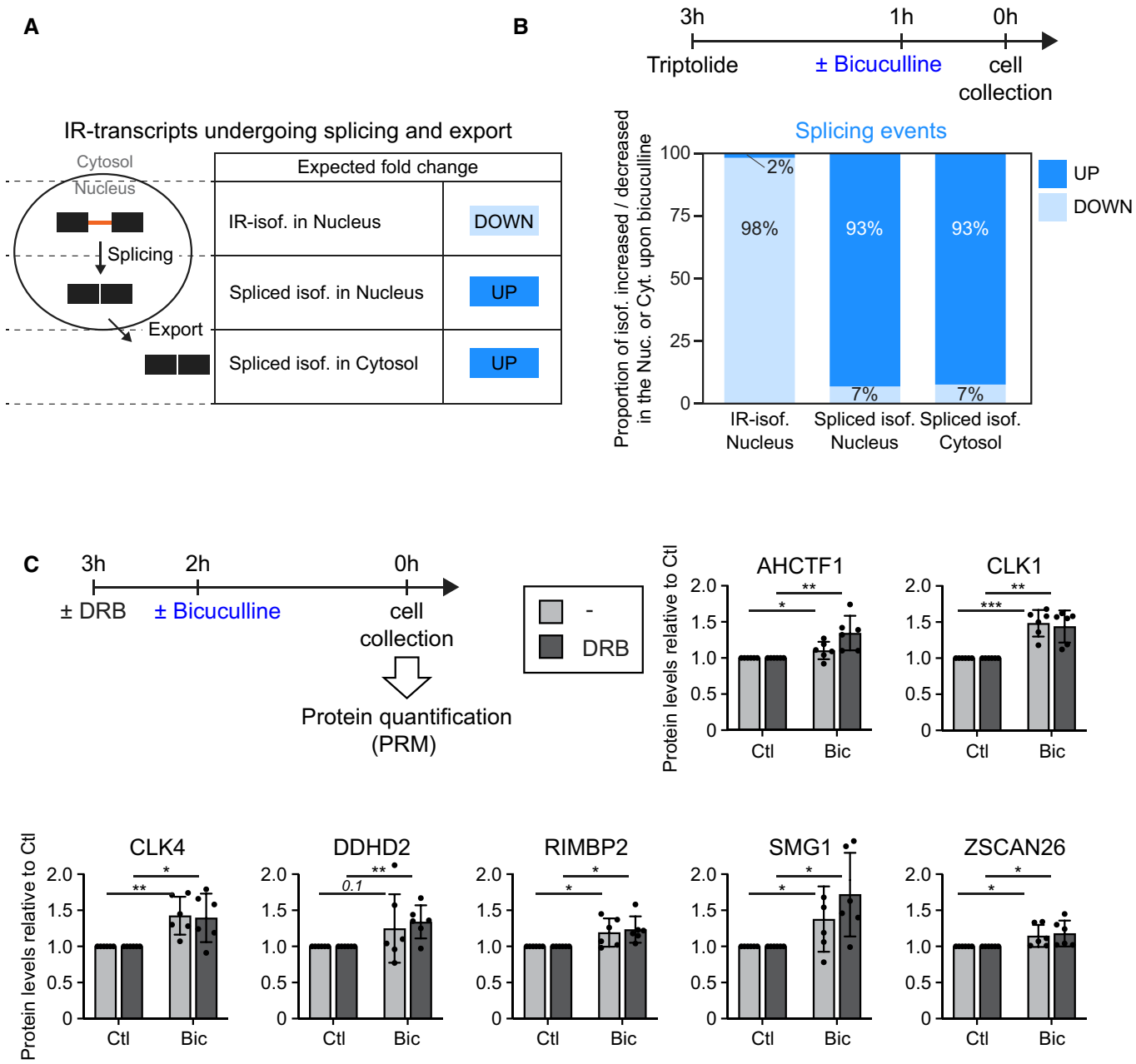

Figure 4. Activity-dependent splicing of intron-retaining transcripts promotes a widespread cytosolic export of fully spliced transcripts.

A Scheme displaying expected regulations of the intron-retaining transcripts and their associated spliced isoforms in the nuclear and cytosolic compartments—in the case of splicing completion and subsequent export in response to stimulation.

B Histogram displaying the actual proportion of IR- and spliced isoforms up- (dark blue) and down- (light blue) regulated in the nucleus and the cytosol. Data are shown for transcripts associated with IRs regulated by splicing in response to bicuculline. In all conditions, Triptolide (1 μM) was applied to mouse primary neocortical cells (14 days in culture) for 3 h; 1 h before cell collection, bicuculline (20 μM) was applied or not (control). Only transcripts that retained an intron in unstimulated-WCE conditions (minPIR ≥ 20) were considered for the analysis. Transcripts were considered regulated through splicing if the followings are applied: (i) IR-transcript expression fold change ≥ 20% and |z-score| ≥ 1.5 in the WCE, (ii) Spliced isoform expression fold change ≥ 20% and |z-score| ≥ 1.5 in the WCE and (iii) expression of the IR- and the spliced isoforms evolved in opposite directions in the WCE (three independent cultures).

C Bar graphs displaying the levels of proteins encoded by seven transcripts containing an IR regulated through splicing upon bicuculline stimulation. In all conditions, DRB (50 μM) was applied to mouse primary neocortical cells (14 days in culture) for 3 h; 2 h before cell collection, bicuculline (20 μM) was applied or not (control). Means and SDs are displayed (six independent cultures); the *P*-values calculated with a one-tailed paired *t*-test are indicated (as numerical values when $P > 0.05$, as * when $P < 0.05$, as ** when $P < 0.01$ and as *** when $P < 0.001$).

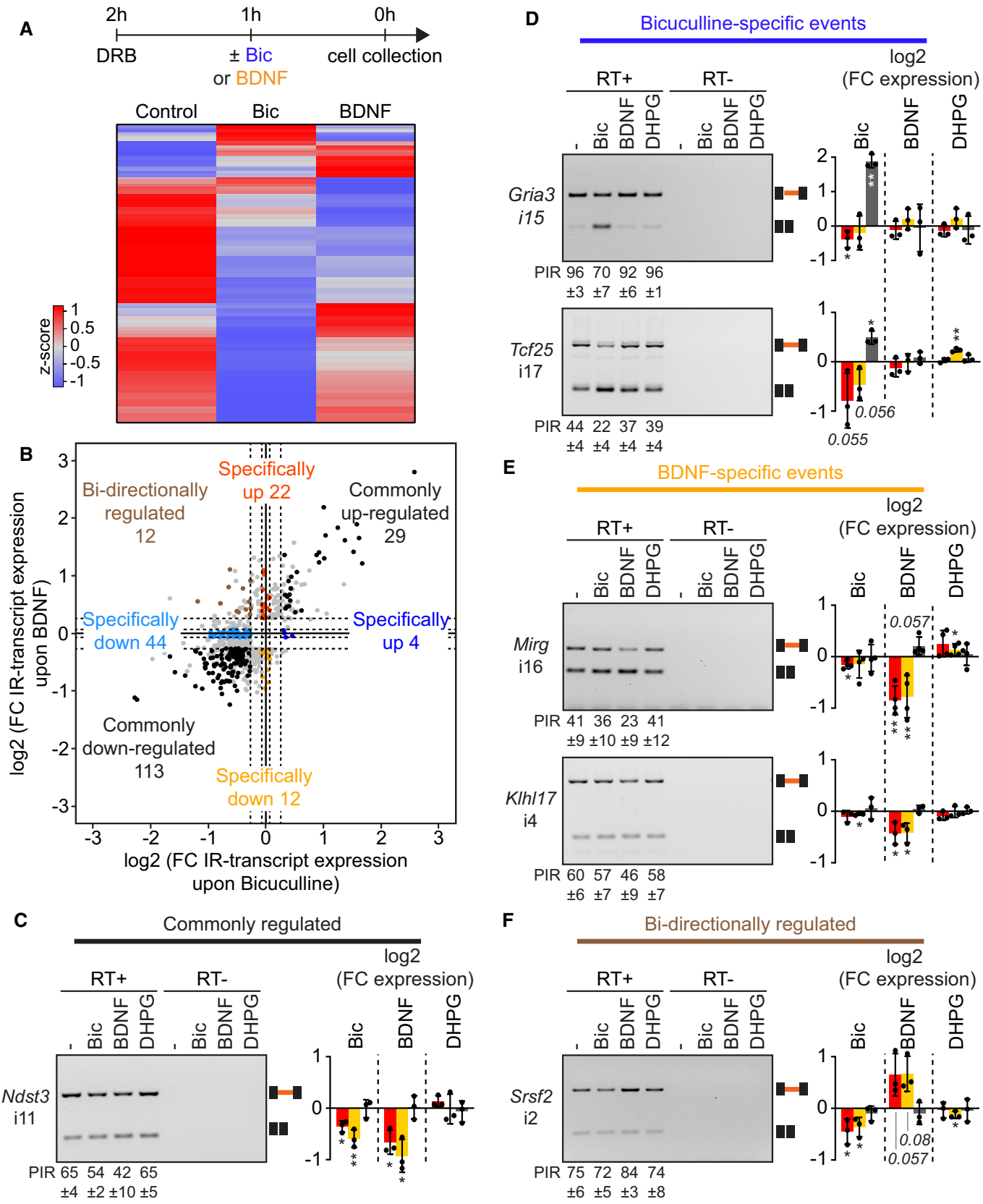
A
2h
1h
0h
DRB
± Bic
or BDNF
cell collection
Control
Bic
BDNF
z-score
1
0.5
0
-0.5
-1
B
Bi-directionally regulated 12
Specifically up 22
Commonly up-regulated 29
Specifically down 44
Specifically up 4
Commonly down-regulated 113
Specifically down 12
log2 (FC IR-transcript expression upon BDNF)
log2 (FC IR-transcript expression upon Bicuculline)
C
Commonly regulated
RT+
RT-
-
Bic
BDNF
DHPG
log2 (FC expression)
Ndst3 i11
PIR 65 54 42 65
±4 ±2 ±10 ±5
D
Bicuculline-specific events
Gria3 i15
PIR 96 70 92 96
±3 ±7 ±6 ±1
Tcf25 i17
PIR 44 22 37 39
±4 ±4 ±4 ±4
0.056
0.055
E
BDNF-specific events
Mirg i16
PIR 41 36 23 41
±9 ±10 ±9 ±12
Klhl17 i4
PIR 60 57 46 58
±6 ±7 ±9 ±7
0.057
F
Bi-directionally regulated
Srsf2 i2
PIR 75 72 84 74
±6 ±5 ±3 ±8
0.08
0.057

Figure 5.

Figure 5. Stimulus-specific regulation of sub-population of intron retentions.

A Heatmap of the IR-transcript expression values in control, bicuculline-stimulated and BDNF-stimulated conditions. IR-transcripts regulated in at least one condition are displayed (fold change of intron-retaining transcript expression ≥ 20% and |z-score| ≥ 1.5).

B Pairwise comparison of the expression fold change (FC) of intron-retaining isoforms upon bicuculline and BDNF stimulation. Every transcript containing a retained intron (minPIR > 20%) in control condition is plotted. IR-transcripts that are considered regulated specifically upon bicuculline (light and dark blue) or BDNF (orange and red) stimulation if the followings are applied: (i) IR-transcript expression fold change ≥ 20% and |z-score| ≥ 1.5 upon bicuculline (or BDNF) stimulation and (ii) IR-transcript expression fold change ≤ 5% upon BDNF (or bicuculline) stimulation. IR-transcripts that are considered commonly regulated upon bicuculline and BDNF stimulation (black) if the followings are applied: (i) IR-transcript expression fold change ≥ 20% and |z-score| ≥ 1.5 upon bicuculline stimulation, (ii) IR-transcript expression fold change ≥ 20% and |z-score| ≥ 1.5 upon BDNF stimulation and (iii) IR-transcripts evolved in the same direction upon bicuculline and BDNF stimulation. IR-transcripts that are considered bi-directionally regulated upon bicuculline and BDNF stimulation (brown) if the followings are applied: (i) IR-transcript expression fold change ≥ 20% and |z-score| ≥ 1.5 upon bicuculline stimulation, (ii) IR-transcript expression fold change ≥ 20% and |z-score| ≥ 1.5 upon BDNF stimulation and (iii) IR-transcripts evolved in opposite directions upon bicuculline and BDNF stimulation.

C–F RT-PCR validations of IR-transcripts are commonly regulated (C), specifically regulated upon bicuculline stimulation (D), specifically regulated upon BDNF stimulation (E) and bi-directionally regulated (F). Expression of the IR-transcripts and the spliced isoforms were analyzed by semi-quantitative PCR (left panels). Means and SDs of PIR values are shown beneath each panel. In addition, fold changes (FC) in the expression of the IR-transcripts (red and orange) and spliced isoforms (dark gray) were assessed with real-time qPCR. Means and SDs are displayed; the *P*-values calculated with a one-tailed paired *t*-test are indicated (as * when $P < 0.05$, as ** when $P < 0.01$, as *** when $P < 0.001$ and as numerical values when *P*-value is close to the 0.05-significance threshold) (3–4 independent cultures).

Remarkably, the application of the selective NMDA receptor antagonist AP5 impaired the bicuculline-dependent intron excision of *Tcf25* and *Gria3* transcripts (Fig 6A and EV6A). Intron excision in these transcripts was also suppressed by pharmacological inhibition (KN-62) of calcium/calmodulin-dependent protein kinases (CaMK)—a downstream mediator activated by NMDAR-dependent calcium entry. By contrast, the MAPK antagonist U0126 did not impact splicing induction of bicuculline-sensitive transcripts. Conversely, for BDNF-sensitive introns, we found that the MAPK pathways are essential for the splicing of *Mirg* and the stabilization of *Srsf2* IR-transcripts upon BDNF stimulation (Fig 6B and EV6B). However, the pharmacological inhibition of NMDA receptors and CaMK pathways did not preclude their regulation upon BDNF stimulation. Overall, these results uncover a signaling pathway specificity of IR programs.

To obtain deeper insight into this cue-specific regulation, we focused on kinases previously implicated in signaling-dependent alternative splicing control (Shin & Manley, 2004). SR-protein kinases (SRPK) and the CDC2-like kinases (CLK) families have previously been shown to link external cues and alternative splicing regulation in non-neuronal cells (Ninomiya *et al*, 2011; Zhou *et al*, 2012). These kinase families both regulate the phosphorylation status—and consequently the activity—of SR proteins, the main family of splicing factors. Interestingly, SRPIN340, a pharmacological inhibitor of SRPK impeded intron excision of *Tcf25* and *Gria3* transcripts upon bicuculline treatment (Fig 6C). However, SPRK inhibition had no effect on the BDNF-dependent splicing of *Mirg* or the BDNF-dependent regulation of *Srsf2* transcripts (Fig 6D). Interestingly, KH-CB19, a pharmacological blocker of CLK kinase activity had no impact on neither bicuculline- or BDNF-dependent introns. Thus, these results further support that the cue-specificity of IR programs strongly relies on the activation of selective signaling pathways transduced to the nucleus to convey the mobilization of distinct sets of IR-transcripts.

In summary, this work identifies selective intron retention and excision programs elicited by distinct forms of neuronal stimulation. The activation of distinct signaling pathways drives the remodeling of the neuronal transcriptome in a cue-specific manner (Fig 6E).

Discussion

In this work, we revealed that regulated intron retention is a widespread, cue-specific mechanism for neuronal transcriptome remodeling. We performed a comprehensive mapping of the subcellular localization of RNAs in mature neurons and revealed that transcripts that stably retain introns are broadly targeted for nuclear retention. We systematically probed these transcripts upon neuronal stimulation and found that sub-populations of nuclear-retained

Figure 6. Stimulation-specificity of intron retention programs is conveyed by distinct signaling pathways.

A, B Analysis of signaling pathways involvement in the regulation of IR-transcripts upon bicuculline (A) and BDNF (B) stimulation. In all conditions, DRB (50 μM) was applied to mouse primary neocortical cells (14 days in culture) for 2 h; 1 h before cell collection, bicuculline (Bic, 20 μM) or BDNF (50 ng/ml) was added to the cultures. 15 min before bicuculline or BDNF stimulation, different pharmacological treatments were applied in order to block NMDA receptors with the antagonist AP5 (50 μM) or the calcium/calmodulin-dependent protein kinases (CaMK) with KN-62 (10 μM) or the mitogen-activated protein kinases (MAPK) with U0126 (10 μM). Fold changes (FC) in the expression of the IR- (red and orange) and spliced (dark gray) isoforms were assessed with real-time qPCR using three different primer sets, as represented in the right scheme. Means and SDs are displayed; the *P*-values calculated with a one-tailed paired *t*-test are indicated (as * when $P < 0.05$, as ** when $P < 0.01$, as *** when $P < 0.001$ and as numerical values when *P*-value is close to the 0.05-significance threshold) (two-to-four independent cultures).

C, D Analysis of SPRK and CLK involvement in the regulation of IR-transcripts upon bicuculline (C) and BDNF (D) stimulation. In all conditions, DRB (50 μM) was applied to mouse primary neocortical cells (14 days in culture) for 2 h; 1 h before cell collection, bicuculline (Bic, 20 μM) or BDNF (50 ng/ml) was added to the cultures. 15 min before bicuculline or BDNF stimulation, different pharmacological treatments were applied in order to block SR-protein kinases (SRPK) with SRPIN340 (10 μM) or CDC2-like kinases (CLK) with KH-CB19 (10 μM). Fold changes (FC) in the expression of the IR- (red and orange) and spliced (dark gray) isoforms were assessed with real-time qPCR using three different primer sets, as represented in the right scheme. Means and SDs are displayed; the *P*-values calculated with a one-tailed paired *t*-test are indicated (as * when $P < 0.05$, as ** when $P < 0.01$, as *** when $P < 0.001$ and as numerical values when *P*-value is close to the 0.05-significance threshold) (two-to-four independent cultures).

E Working model. Selective IR programs—elicited upon distinct forms of neuronal stimulation and the subsequent activation of signaling pathways—remodel neuronal transcriptome in a cue-specific manner.

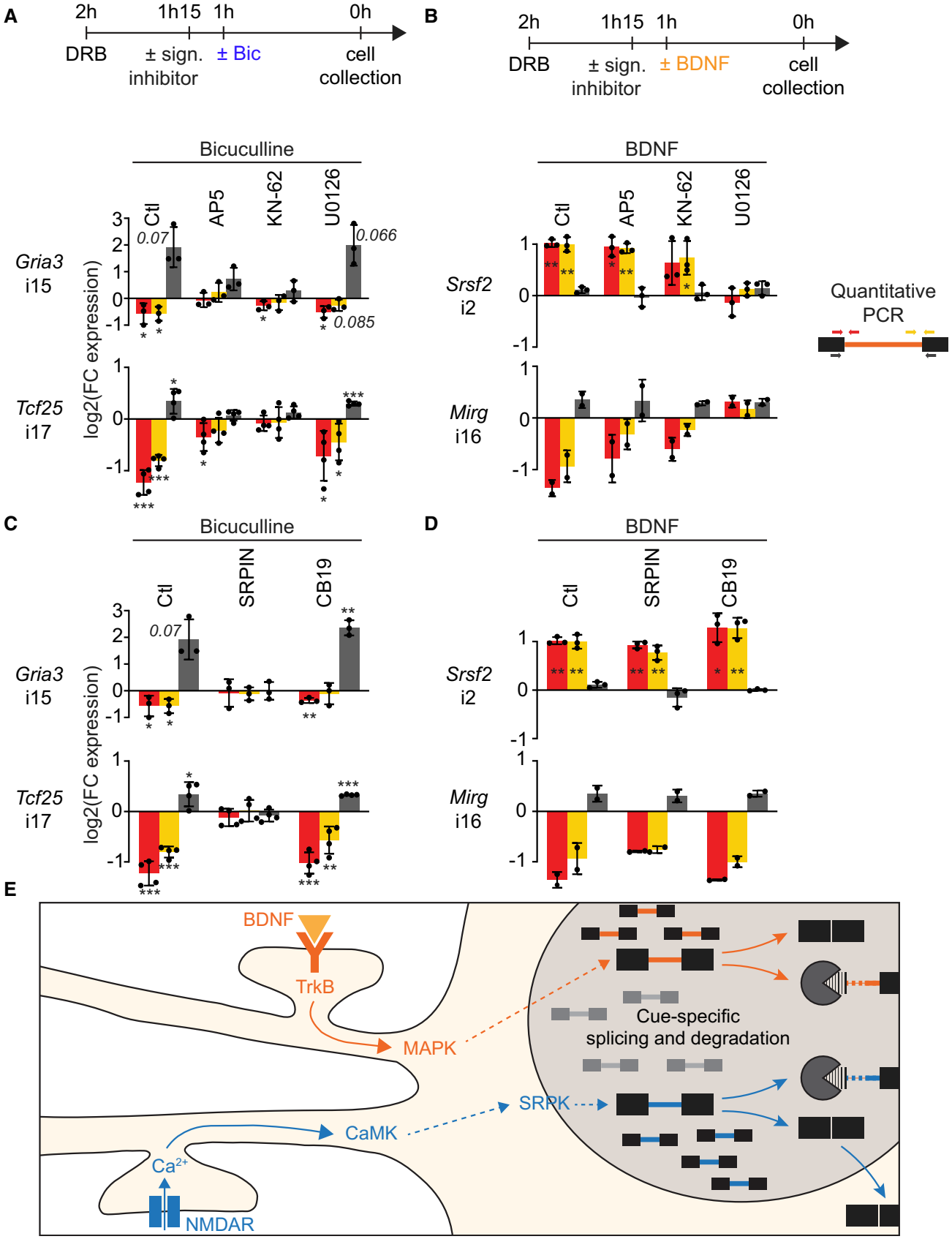
A
2h
1h15
1h
0h
DRB
± sign. inhibitor
± Bic
cell collection
B
2h
1h15
1h
0h
DRB
± sign. inhibitor
± BDNF
cell collection
Bicuculline
BDNF
Ctl
AP5
KN-62
U0126
Gria3 i15
Tcf25 i17
Srsf2 i2
Mirg i16
log2(FC expression)
0.07
0.066
0.085
Quantitative PCR
C
D
SRPIN
CB19
E
BDNF
TrkB
MAPK
CaMK
SRPK
Ca2+
NMDAR
Cue-specific splicing and degradation

Figure 6.

transcripts are bi-directionally regulated in response to several cues: some appear targeted for degradation while others undergo splicing completion to generate fully mature mRNAs. This latter set of transcripts is exported to the cytosol and used for a rapid production of associated proteins. Remarkably, distinct groups of IR-transcripts are regulated depending on the form of stimulation and this selectivity arises from the activation of specific signaling pathways. Overall, our data identifies IR as a major regulator of nuclear mRNA retention and cue-specific gene expression.

Stable intron-retaining transcripts are mainly localized in the nucleus

In the present study, we systematically analyzed the localization of stable intron-retaining transcripts. We found that the majority of intron-retaining transcripts are present in the nucleus (Fig 1B–D). This is consistent with previous candidate gene studies in neurons and other cell classes, including fibroblastic cells, stem cells and male gametes, which reported nuclear localization of individual IR-transcripts. (Ninomiya *et al*, 2011; Boutz *et al*, 2015; Mauger *et al*, 2016; Naro *et al*, 2017). Previous work also showed that instable IR-transcripts are mainly localized in the nucleus (Braunschweig *et al*, 2014). This highlights that the nuclear localization *per se* of intron-retaining transcripts does not dictate their fate towards storage or degradation. Some studies revealed factors important for targeting intron-retaining transcripts to degradation in the nucleus (Kilchert *et al*, 2015). Moreover, early studies showed that loading of some spliceosome factors onto pre-RNAs prevents their export to the cytosol (Chang & Sharp, 1989; Legrain & Rosbash, 1989). Likewise, the recruitment of some spliceosome components onto intron-retaining transcripts could explain their nuclear retention. Whether a partial spliceosome assembly onto intron-retaining transcripts protects them from nuclear degradation remains to be investigated.

Interestingly, while most stable intron-retaining transcripts are found in the nucleus, we also observed a notable fraction of them in the cytosol (Fig 1B–D). Some of them could act as alternative coding isoforms to increase proteome diversity (Grabski *et al*, 2021). Alternatively, such cytoplasmic forms might have non-protein coding functions. For instance, intron-retaining *Camk2a* transcripts and the 3′UTR-intron-containing *Calm3* isoforms are localized in the cytoplasm of neuronal processes; however these transcripts do not appear to be translated (Ortíz *et al*, 2017; Sharangdhar *et al*, 2017). Remarkably, dendritic localization of *Camk2a* and *Calm3* is regulated by neuronal activity. While the biological function remains elusive, these transcripts have been hypothesized to act as sponges for miRNAs and RNA-binding proteins, thus locally regulating their actions. Interestingly, we found that non-regulated retained introns exhibit a strong bias for the 3′ end of the transcripts (Fig EV2F) suggesting that alike *Calm3*, many transcripts contain a 3′UTR-intron. It will be interesting to probe whether all of these transcripts are localized in the neuronal processes or whether a sub-category remains in the nucleus.

Intron retention is associated with an acute mobilization of mRNAs in the cytosol and an increase of protein levels

Our data support that regulated intron retention and excision is a widespread mechanism to control transcript localization and protein expression. The nuclear localization of transcripts that stably retain select introns makes them unavailable for protein synthesis (Fig 1B–D). Importantly, in response to neuronal stimulation, we found that the subsets of transcripts completing their splicing are significantly increased in the cytosol supporting their widespread activity-dependent export (Fig 4B). In addition, we shed light on a rapid elevation of the corresponding protein products (Fig 4C). Thereby, we hypothesize that regulation of IRs represents a mechanism to rapidly modify the neuronal proteome which contributes to activity-dependent plasticity. Notably, an elevation of the neuronal network excitation rapidly induces an increase of RIMBP2 (Fig 4C), a component of the pre-synaptic active zone that plays a crucial role in neurotransmission in various synapses (Liu *et al*, 2011; Brockmann *et al*, 2019). Strikingly, we also found that in response to neuronal stimulation, several gene expression regulators including the transcription factor AHCTF1, the splicing regulators CLK1/4 and the nonsense-mediated decay factor SMG1, are up-regulated (Fig 4C). These factors are well positioned to trigger profound activity-dependent neuronal transcriptome remodeling. Thus, targeted intron retention and excision upon stimulation could contribute to plasticity and learning. Interestingly, in *Drosophila*, learning paradigms elevate the spliced isoform of *Orb2A* mRNA—encoding a protein involved in memory consolidation—over an unspliced isoform that is predominant in naive flies (Gill *et al*, 2017).

Noteworthy, we also identified some non-protein coding RNAs containing a regulated IR. Notably, the miRNA containing gene Mirg —whose deletion is associated with synaptic transmission and social behavior alterations (Marty *et al*, 2016; Lackinger *et al*, 2019) —is expressed as an intron-retaining transcript that completes its splicing in response to BDNF stimulation (Fig 3D). Thus, crosstalk between IR and Mirg might represent a mechanism to regulate the expression of miRNAs in response to neuronal cues.

Other studies revealed a link between IR or spliced isoforms profile and the respective nuclear versus cytosolic localization of their host transcripts (Ninomiya *et al*, 2011; Boutz *et al*, 2015; Mauger *et al*, 2016; Naro *et al*, 2017; Yeom *et al*, 2021). Though, in most of the cases, it was unclear (i) whether existing transcripts redirect their fate and localization through splicing completion or (ii) whether co-transcriptional production of spliced isoforms is required for their cytosolic expression. Indeed, the fate and nuclear localization of some IR-transcripts can be irreversibly set up during the transcription stage (Park *et al*, 2017; Pendleton *et al*, 2017, 2018). By contrast, we show here that a sizeable population of IR-transcripts can redirect their fate post-transcriptionally upon environmental signals and promote their release into the cytosol. Such a transcription-independent mechanism likely evolved to facilitate rapid remodeling of the transcriptome, independently of transcription which is time-limiting due to the finite processivity of the RNA-polymerase II (Tennyson *et al*, 1995; Darzacq *et al*, 2007; Singh & Padgett, 2009; Fuchs *et al*, 2014; Veloso *et al*, 2014).

Intron retention programs remodel the neuronal transcriptome in a cue-specific manner

Previous studies showed that IR profiles across tissues and cell types are modified by numerous signals including cellular differentiation, neuronal stimulation, metabolic homeostasis and cellular stress

(Wong *et al*, 2013; Boutz *et al*, 2015; Mauger *et al*, 2016; Pimentel *et al*, 2016; Quesnel-Vallières *et al*, 2016; Naro *et al*, 2017; Park *et al*, 2017; Parra *et al*, 2018; Pendleton *et al*, 2018; Green *et al*, 2020; Haltenhof *et al*, 2020). But it has remained unclear whether in the same cellular system IRs could be differentially regulated upon distinct signals. In the present work, we unveil that in mature neurons, IR programs are cue-specific. Selectivity arises from the activation of distinct neuronal signaling pathways (Figs 5 and 6) and distinct subsets of IR-transcripts are regulated in response to specific neuronal stimuli (Fig 5). We did not identify any enriched RNA sequence motifs dictating the selective fate of intron towards distinct stimuli; thus, further studies will be required to decipher the RNA factors controlling the cue-specificity of IR regulation.

We hypothesize that selective intron retention and excision programs confer a rapid and cue-specific way to induce molecular signatures in stimulated neurons. Similarly, activity-dependent transcriptional programs (Chen *et al*, 2016; Yang *et al*, 2016; Tyssowski & Gray, 2019) and local translation programs (Cagnetta *et al*, 2018) exhibit a high cue-specificity which is thought to trigger specific plasticity events. To conclude, this study reveals that regulated intron retention and excision mechanism is well positioned to instruct rapid and cue-specific plasticity events. This gives new insights to understand molecular determinants underlying higher cognitive functions—such as learning—that involve the integration of multiple and diverse stimuli.

Materials and Methods

Primary neocortical cultures and pharmacological treatments

All procedures related to animal experimentation were reviewed and approved by the Kantonales Veterinäramt Basel-Stadt. Swiss mice (Janvier) were group housed (weaning at postnatal day 21–23) under a 12-h light/dark cycle (06:00–18:00) with food and water ad libitum. Dissociated cultures of neocortical cells were prepared from E16.5 mouse embryos (embryonic stage 16.5). Neocortices were dissociated by the addition of papain (130 units, Worthington Biochemical, LK003176) for 30 min at 37°C. Cells (45,000 cells/cm^2) were maintained in neurobasal medium (Gibco, 21103-049) containing 2% B27 supplement (Gibco, 17504-044), 1% Glutamax (Gibco, 35050-61), and 1% penicillin/streptomycin (Bioconcept, 4-01F00-H) for 14 days. The following reagents for pharmacological treatments were used (at the indicated concentrations and from the stated sources): DRB (50 μM, Sigma, D1916), triptolide (1 μM, Sigma, T3652), bicuculline (20 μM, Tocris, 0130), BDNF (50 ng/ml, Sigma, B7395), DHPG (10 μM, Tocris, 0805), DL-AP5 (50 μM, Tocris, 3693), KN-62 (10 μM, Tocris, 1277), U0126 (10 μM, Tocris, 1144), SRPIN340 (10 μM, Tocris, 5063) and KH-CB19 (10 μM, Tocris, 4262).

Cellular fractionation

Cell fractionation experiments were performed according to the protocol from Suzuki *et al* (2010). Briefly, two million cells plated in a 10-cm^2 dish were collected in ice-cold PBS. After 10 s-centrifugation, the supernatant was removed from each sample and the cell pellet was resuspended in 450 μl ice-cold 0.1% NP40 in PBS. One aliquot was collected as the whole cell extract and then the leftover was spun for 10 s. The supernatant was collected as the cytosolic-enriched fraction and the pellet (after one wash with 450 μl 0.1% NP40 in PBS) as the nuclear-enriched fraction.

Western blot and antibodies

Total proteins were separated by electrophoresis on 4–20% gradient PAGE gels (Bio-Rad, 4561093) and transferred onto nitrocellulose membrane. The following antibodies were used: anti-phosphoAKT (Ser473) (Cell Signaling, 9271S), anti-AKT (Cell Signaling, 9272S), anti-phosphoCREB (Ser133) (Millipore, aa77-343), anti-phosphoERK (Cell signaling, 4370S), anti-ERK (Cell signaling, 4695S), anti-phospho-CTD RNA polymerase II (Ser2) (Abcam, ab5095), anti-CTD RNA polymerase II (Abcam, ab817), anti-N-terminal RNA polymerase II A-10 (Santa Cruz, sc17798), anti-ACTININ (Abcam, ab68194), anti-COFILIN (Abcam, ab54532), anti-GAPDH (clone D16H11, Cell Signaling, 5174), anti-MECP2 (Cell Signaling, 3456), anti-U1-70K (clone H111, Synaptic Systems, 203011), anti-LAMIN B1 (Abcam, ab133741), anti-hnRNPA1 (clone D21H11, Cell Signaling, 8443), and anti-betaIII TUBULIN (Abcam, ab18207).

Targeted mass spectrometry

Totally 500,000 cells were collected and lysed in 200 μl lysis buffer (1% sodium deoxycholate (SDC), 0.1 M TRIS, 10 mM TCEP, pH = 8.5) using strong ultra-sonication (10 cycles, Bioruptor, Diagnode). Protein concentration was determined based on the measurement of tryptophan fluorescence in the samples (Wiśniewski & Gaugaz, 2015). Sample aliquots containing 50 μg of total proteins were reduced for 10 min at 95°C and alkylated at 15 mM chloroacetamide for 30 min at 37°C. Proteins were digested by incubation with sequencing-grade modified trypsin (1/50, w/w; Promega, Madison, Wisconsin) overnight at 37°C. Peptides were then cleaned up using iST cartridges (PreOmics, Munich) according to the manufacturer's instructions. To each peptide sample, an aliquot of a heavy reference peptide mix containing chemically synthesized proteotypic peptides (Spike-Tides, JPT, Berlin, Germany) was spiked into each sample at a concentration of 2 fmol of heavy reference peptides per 1 μg of total endogenous protein mass. Samples were dried under vacuum and stored at −20°C until further use.

Peptides were resuspended in 0.1% aqueous formic and peptide concentration was adjusted to 0.25 μg/μl. A 1 μL of each sample was subjected to LC–MS/MS analysis using an Orbitrap Eclipse Tribrid Mass Spectrometer fitted with an Ultimate 3000 nano system (both Thermo Fisher Scientific) and a custom-made column heater set to 60°C. Peptides were resolved using an RP-HPLC column (75 μm × 30 cm) packed in-house with C18 resin (ReproSil-Pur C18–AQ, 1.9 μm resin; Dr. Maisch GmbH) at a flow rate of 0.3 μl/min. The following gradient was used for peptide separation: from 2% B to 35% B over 55 min, to 50% B over 5 min, to 95% B over 2 min followed by 11 min at 95% B then back to 2% B. Buffer A was 0.1% formic acid in water and buffer B was 80% acetonitrile, 0.1% formic acid in water. For PRM-MS analysis (MS2 scan), the resolution of the orbitrap was set to 120,000 FWHM (at 200 m/z), isolation window was set to 0.4 m/z, normalized AGC target was set to 2000% and maximum injection time was 246 ms. For each MS cycle, a full MS1 scan at 60,000 FWHM (at 200 m/z) was

included. Targeted peptide panel was split into 2 injections and PRM isolations were scheduled with the 5 min retention time window. In addition, few selected samples were also analyzed in DDA mode using the same LC gradient as above.

The PRM files were processed using Skyline software (v. 21.2.0.425). Up to 6 most intense transitions per peptides were selected and peptides light-to-heavy ratios were exported. Only peptides with DotProductLightToHeavy ratios higher than 0.8 were considered for quantitative analysis. To control for variation in injected sample amount, the MS1 signal of PRM samples was aligned with DDA runs using Progenesis QI software (Nonlinear Dynamics, Version 2.0). Extracted peptide precursors were exported as .mgf files and were searched using MASCOT against a murine database. Search results were imported back to Progenesis and the sum of raw peptide intensities per injection was used for normalization.

Immunocytochemistry and image analysis

For immunocytochemistry, mouse primary neocortical neurons were fixed with 4% PFA in 1X PBS for 15 min. Cells were then permeabilized with ice-cold methanol for 10 min and blocked (5% donkey serum, 0.03% Triton X-100 in 1X PBS) for 1 h at room temperature. Primary antibody incubation was performed overnight at 4°C in a humidified chamber. Secondary antibody incubation was then performed for 1 h at room temperature. The following antibodies were used: anti-phosphoERK (Cell signaling, 4370S), anti-MAP2 (Synaptic systems, 188004), Cy5-conjugated donkey anti-guinea pig (Jackson, 706-715-148) and Cy3-conjugated donkey anti-rabbit (Jackson, 711-165-152). Imaging was performed on a widefield microscope (FEI MORE) with a 40X objective (NA 0.95, air). Image analysis was performed on Fiji (Schindelin *et al*, 2012). Briefly, a mask for MAP2 signal was created and neuronal cell bodies were manually delimited. The mean of phospho-ERK signal intensity for each neuronal cell body was then measured.

RNA isolation and reverse transcription

Cells were lysed using Trizol reagent (Sigma, T9424). Total RNAs were isolated and DNase treated on columns (RNeasy micro kit, Qiagen, 74004) following the manufacturer's instructions. The cDNA libraries were built using between 100 and 500 ng RNA reverse transcribed with SuperScript III reverse transcriptase (Thermo Fisher, 18080044), dNTPs (Sigma, D7295) and oligo$(dT)_{15}$ primer (Promega, C1101).

PCR

Semi-quantitative PCR was performed using Phusion High-Fidelity DNA Polymerase (New England Biolabs, M0530L) and revealed with GelRed (Biotium, 41003). For each PCR, the number of cycles necessary to end the amplification in its exponential phase was determined. In the case of long introns (> 1,000–1,500 bp), multiplex PCRs were performed to amplify both the intron-retaining and the spliced transcript isoforms (i.e., using three primers: one primer complementary to an internal region of the intron in addition to the primers mapping to each flanking exon).

Real-time quantitative PCRs were performed with FastStart Universal SYBR GreenMaster (Roche, 04-913-850-001). PCRs were carried out in a StepOnePlus qPCR system (Applied Biosystems) with the following thermal profile: 10 min at 95°C, 40 cycles of 15 s at 95°C and 1 min at 60°C. Real-time quantitative PCR assays were analyzed with the StepOne software. The primers used for PCRs are listed in Table 2.

Deep RNA-sequencing

RNA samples were quality-checked on the TapeStation instrument (Agilent Technologies) using the RNA ScreenTape (Agilent, 5067-5576) and quantified by Fluorometry using the QuantiFluor RNA System (Promega, E3310). Library preparation was performed, starting from 200 ng total RNAs, using the TruSeq Stranded mRNA Library Kit (Illumina, 20020595) and the TruSeq RNA UD Indexes (Illumina, 20022371). Fifteen cycles of PCR were performed. Libraries were quality-checked on the Fragment Analyzer (Advanced Analytical) using the Standard Sensitivity NGS Fragment Analysis Kit (Advanced Analytical, DNF-473) revealing an excellent quality of libraries (average concentration was 158 ± 20 nmol/L and average library size was 351 ± 6 base pairs). Samples were pooled to equal molarity. The pool was quantified by Fluorometry using the QuantiFluor ONE dsDNA System (Promega, E4871). Libraries were sequenced Paired-End 101 bases using the HiSeq 2500 or NovaSeq 6000 instrument (Illumina) and the S2 Flow-Cell loaded. Details on the number of sequenced reads for each sample are given in Table 1. Quality control of read sequences was performed in collaboration with the company GenoSplice technology (http://www.genosplice.com). Confidence score per base and per sequence, GC content, sequence length, adapter content and presence of overrepresented sequences were assessed using FAST-QC.

RNA-sequencing read alignment

For the RNA-sequencing data analysis, reads were aligned onto the mouse genome assembly mm10 using the STAR aligner version 2.4.0f1 (Dobin *et al*, 2013). The following parameters were used: –outFilterMismatchNmax 2 and –outFilterMultimapNmax 1 to filter out reads that have more than two mismatches and reads that map to multiple loci in the genome. Moreover, reads with < 8 nt overhang for the splice junction on both sides were filtered out using –outSJFilterOverhangMin 30 8 8 8. Then, read alignment files (bam) were processed with custom Perl scripts using the library Bio::DB::Sam. For each segment comprising a pair of consecutive exons (exon1 and exon2) and the intermediate intron, reads that mapped (i) exon1-intron junctions, (ii) intron-exon2 junctions (iii), exon1-exon2 junctions and (iv) introns were counted.

PIR, intron-retaining isoform expression and spliced isoform expression

For each segment in the mouse genome, comprised of a pair of consecutive exons and the intervening intron annotated in FastDB (http://www.easana.com) (de la Grange *et al*, 2005), we assessed the expression level of transcripts retaining the intron (IR-isoforms) as the average number of reads mapping the 5′ and 3′ exon-intron junctions (= mean(cov(E1I), cov(IE2))). The expression level of the

Table 2. Primer sequences.

	Gene	Intron	Analyzed junction	Forward/Reverse	Sequences
Real-time quantitative PCR primers	Hprt		EE	F	GATGAACCAGGTTATGACCTAGATTTGTTT
				R	ATGGCCTCCCATCTCCTTCAT
	Gria3	i15	EI	F	CAGAGCTACAGAAAGAACAGCAGGAG
				R	GACAGTGTGGTTCTACAACCTCTTCAA
			IE	F	CAGGTTGCCTGCAGTGTCTAAA
				R	CGGAGTCCTTGGCTCCACATT
			EE	F	CAGAGCTACAGAAAGAACAGCAGGAG
				R	CGGAGTCCTTGGCTCCACATT
	Tcf25	i17	EI	F	CACGGAAACACAATCGCCCTCTTCTT
				R	GCCCACACCACTCACCTTAGAATAG
			IE	F	CCCACTTAGCTGTGTCTCATTGTTCAG
				R	CTCCAGGTCGTTGAAGTGGAAGTT
			EE	F	CACGGAAACACAATCGCCCTCTTCTT
				R	TCCAGCCTCTCCCCCTCTGTGG
	Mirg	i16	EI	F	AGGTTGTCTGTGATGAGTTCGCTTTA
				R	GGAAGCCTTAGACAGGGACAAACA
			IE	F	CCTACGTGTGGTAAAGCGGAAACA
				R	ATAGGCAGGGTTCCTTGAACATCC
			EE	F	AGGTTGTCTGTGATGAGTTCGCTTTA
				R	ATAGGCAGGGTTCCTTGAACATCC
	Fnbp4	i11	EI	F	GCAGAAGTGAATGAAGAACAAGATTA
				R	AAAGAGCAAAGATTTCAAATAACGAAA
			IE	F	GTGTCTCTGTAGGAGAACAGATTT
				R	GACTCTCATCTCTAACTTCCTTTGT
			EE	F	GCAGAAGTGAATGAAGAACAAGATTA
				R	GACTCTCATCTCTAACTTCCTTTGT
	Ccdc136	i15	EI	F	GTGAGACCCTTCACAGGAGCTATG
				R	ACCTTCCCTGCCTGACCAATAA
			IE	F	CCAGAGGTGTAGAGTGTAGGACAGA
				R	CTCTTCCTGGCTCACTTGGTACAG
			EE	F	CCAGCAGCACAAGTGTGAGCTATAA
				R	ACTGTTTCCTCAAAGTGCTCCAAGTC
	Klhl17	i4	EI	F	CATTCGAGGATTTGCAGACACACAC
				R	CAAACTGGCATGTTACCTGCTTCAG
			IE	F	GCACATGCCCTCTGTCTGATACT
				R	CGTTCAGGCTATCACTAGAGACCAATTC
			EE	F	CATTCGAGGATTTGCAGACACACAC
				R	CCAATTCCAGCACCTGCTTCAG
	Smg1	i44	EI	F	GGGTGTAACTGGAGTAGAAGGTGTTT
				R	TCAGTAAACTCAACACAAGTTTCCA
			IE	F	CATATGGAAACTTGTGTTGAGTTTACTG
				R	TTCCATCTCTCGCTTACTCTGCTTG
			EE	F	TGTGAGCAGGTTCTCCACATCAT
				R	TTCCATCTCTCGCTTACTCTGCTTG
	Srsf2	i2	EI	F	CTCCAGAAGAAGAGGGAGCAGTTTC

Table 2 (continued)

	Gene	Intron	Analyzed junction	Forward/Reverse	Sequences
				R	AGCATCACTCCCAAAGCTGAGTAA
			IE	F	GCTGTTTCATGCTGTTTGAGACCTATT
				R	CCTGGAGGATCAGCCAAATCAGTTA
			EE	F	CTGCCCGAAGATCCAAGTCCAAGTC
				R	CAGGAGACCGCAGCATTTTCTTAGGAAG
	Ndst3	i11	EI	F	AAATCCTTTGAGGAGGTACAGTTCTTT
				R	TGTGTGGCATGAATGTTATCTGTAGT
			IE	F	TCAGTCACCAGCATATAAACGTAAGGG
				R	GGAGCGTCCTCTGAATGGAAGTAA
			EE	F	AAATCCTTTGAGGAGGTACAGTTCTTT
				R	GGAGCGTCCTCTGAATGGAAGTAA
	Gria2	i14	EI	F	GGAGTCACATTCAAGACACTGTTATTTGTT
				R	AATCTGAATCTTTGGGTAAGGTGGTAGAG
			IE	F	GCTCACCCTGTCTGACAAGTATGTT
				R	ACTCTCCTTTGTCGTACCACCATTT
			EE	F	TTGTTGTGGATAAATGCGGTTAACC
				R	CTCTCCTTTGTCGTACCACCATTTG
	Cdr1os (C230004F18Rik)	i4	EI	F	ACATCGCTGTGGTCCATCTCTATTTAC
				R	ACTGGGATGGAGTAAAGGGTGAAAC
			IE	F	TCTATGTTGTGCAGAGTTACCTTATTACAC
				R	TGTATCTCTGCTGTAGGCCAGAATTG
			EE	F	ACATCGCTGTGGTCCATCTCTATTTAC
				R	TGTATCTCTGCTGTAGGCCAGAATTG
Semi-quantitative PCR primers	Gria3	i15		F	CAGAGCTACAGAAAGAACAGCAGGAG
				R	CGGAGTCCTTGGCTCCACATT
				R	TTTCCCACCCTGTTCCACCAA
	Tcf25	i17		F	CTTCCGGTCCTTGTTGCCAAATTAC
				R	CTCCAGGTCGTTGAAGTGGAAGTT
	Mirg	i16		F	AGGTTGTCTGTGATGAGTTCGCTTTA
				R	ATAGGCAGGGTTCCTTGAACATCC
				R	GGAAGCCTTAGACAGGGACAAACA
	Fnbp4	i11		F	CCTCTGGAAGCAACTACTCCTGATTAAC
				R	TCGCCCGACTGTTCGTTTACATAG
	Ccdc136	i15		F	GTGAGACCCTTCACAGGAGCTATG
				R	CTCTTCCTGGCTCACTTGGTACAG
	Klhl17	i4		F	CATTCGAGGATTTGCAGACACACAC
				R	CGTTCAGGCTATCACTAGAGACCAATTC
	Hprt	EE		F	GATGAACCAGGTTATGACCTAGATTTGTTT
				R	ATGGCCTCCCATCTCCTTCAT
	Srsf2	i2		F	CTCCAGAAGAAGAGGGAGCAGTTTC
				R	CCTGGAGGATCAGCCAAATCAGTTA
	Ndst3	i11		F	AAATCCTTTGAGGAGGTACAGTTCTTT
				F	TTTGCACAGGAGCTAAGGTTTGATTATT
				R	GGAGCGTCCTCTGAATGGAAGTAA

EE, exon-exon junction; EI, 5′ exon-intron junction; IE, 3′ intron-exon junction.

spliced isoform was estimated as the number of exon-exon junction reads (= cov(E1E2)). Given that coverage (cov) is by definition normalized by the length of the analyzed sequence, cov is corresponding to the absolute number of reads mapping a junction. All the read coverage values were normalized by the number of total mapped reads for each individual sample. Segments were considered as non-expressed and filtered out if (cov(E1E2) + mean(cov(E1I), cov(IE2)) < 10) in at least one sample. Note that, for the cell fractionation samples, the segment expression filter only applied to WCE condition. Also, segments whose spliced isoforms were not significantly expressed in any of the compared samples were filtered out: (cov(E1E2) < 10). Again, for cell fractionation samples, this filter only applied to WCE condition. The PIR was then calculated as the expression level of the IR-isoforms over the sum of the expression levels of the IR-isoforms and the spliced isoforms (PIR = mean(cov(E1I), cov(IE2))/(cov(E1E2) + mean(cov(E1I), cov(IE2)))). We defined introns as retained if their PIR exceeded 20 and if they fulfilled the following criterion: the read coverage along the entire intron must represent at least 20% of the sum of the expression of the spliced and IR-isoforms (minPIR = (min(cov(E1I), cov(IE2), cov(I))/(cov(E1E2)) + mean(cov(E1I), cov(IE2); min = minimum)). In this way, we ensured that reads mapping the exon-intron junctions were indeed due to IR rather than other events, such as the usage of alternative 5′ or 3′ splice sites.

Analysis of intron-retaining transcript subcellular localization and spike-in RNAs

Because the quantity of RNAs in the "Nucleus" and the "Cytosol" fractions are not equal, the real enrichment of a given transcript in the nucleus versus the cytosol is lost during the RNA sequencing library preparation. To overcome this hurdle, we added a defined amount of spike-in RNAs SIR-Set3 (Lexogen, Iso Mix E0/ERCC #051) in each fraction arising from a constant number cells before adjusting the RNA quantities during library preparation. Note that we put twice less spike-in RNAs for the nuclear samples. For our analysis, we only considered ERCC that are covered by > 10 reads in every sample (18 ERCCs). We then calculated the cytosol-to-nucleus abundance ratio of each ERCCs. A correction factor was then assessed as the mean of cytosol-to-nucleus ratio for all ERCCs (1.03 ± 0.07). Given that we introduce twice less spike-ins in the nuclear samples, the final correction factor used in this study is 0.515 (=1.03/2). We applied this factor to the RNA sequencing data to calculate a true nucleus-to-cytosol enrichment. IR-transcripts were considered enriched (i) in the nucleus if (mean IR-isoform $\text{expression}_{\text{nucleus}}$/mean IR-isoform $\text{expression}_{\text{cytosol}} \geq 2$) or (ii) in the cytosol if (mean IR-isoform $\text{expression}_{\text{nucleus}}$/mean IR-isoform $\text{expression}_{\text{cytosol}} \leq 0.5$). For the evaluation of splice-site strength, maximum entropy scores for 9-bp 5′ splice sites and 20-bp 3′ splice sites were calculated using MaxEntScan (Yeo & Burge, 2004).

Analysis of stimulation-dependent intron-retaining transcripts

Intron-retaining transcripts were considered as regulated if the following criteria applied: (i) the fold change mean of IR-transcript expression (FC IR expression) ≥ 20%, and (ii) |z-score| of IR-transcript expression ($|\text{z-score}|_{\text{IR expression}}$) ≥ 1.5, where z-score = ((mean IR $\text{expression}_{\text{stimulated}}$ − mean IR $\text{expression}_{\text{unstimulated}}$)/sqrt(paired variance IR expression)) and paired variance IR expression = (var(IR $\text{expression}_{\text{unstimulated}}$) + var(IR $\text{expression}_{\text{stimulated}}$) − 2 × covar(IR expression)).

For all regulated intron-containing transcripts, the stimulation-specificity was defined as follows: commonly regulated IRs: (i) FC IR expression ≥ 20% upon both bicuculline and BDNF stimulation, (ii) IRs regulated in the same direction upon both bicuculline and BDNF stimulation, (iii) $|\text{z-score}|_{\text{IR expression}} \geq 1.5$ upon both bicuculline and BDNF stimulation; differentially regulated IRs: (i) FC IR expression ≥ 20% upon both bicuculline and BDNF stimulation, (ii) IRs regulated in opposite directions upon bicuculline and BDNF stimulation, and (iii) $|\text{z-score}|_{\text{IR expression}} \geq 1.5$ upon both bicuculline and BDNF stimulation; bicuculline-specific IRs: (i) FC IR expression ≥ 20% upon bicuculline stimulation, (ii) $|\text{z-score}|_{\text{IR expression}} \geq 1.5$ upon bicuculline stimulation, and (iii) FC IR expression ≤ 5% upon BDNF stimulation; BDNF-specific IRs: (i) FC IR expression ≥ 20% upon BDNF stimulation, (ii) $|\text{z-score}|_{\text{IR expression}} \geq 1.5$ upon BDNF stimulation, and (iii) FC IR expression ≤ 5% upon bicuculline stimulation. For regulated intron-containing transcripts that do not belong to one of these groups, we considered we could not confidently determine their stimulation-specificity.

To probe by which RNA process IR-transcripts are regulated, we used the following criteria for the spliced isoform: splicing: (i) fold change mean of spliced isoform expression (FC SI expression) ≥ 20%, (ii) $|\text{z-score}|_{\text{SI expression}} \geq 1.5$ (where z-score = ((mean SI $\text{expression}_{\text{stimulated}}$ − mean SI $\text{expression}_{\text{unstimulated}}$)/sqrt(paired variance SI expression)) and paired variance SI expression = ((var(SI $\text{expression}_{\text{unstimulated}}$) + var(SI $\text{expression}_{\text{stimulated}}$) − 2 × covar(SI expression))), and (iii) SI regulated in opposite directions compared to IR-isoforms; degradation/stabilization: (i) FC SI expression ≤ 5% and (ii) $|\text{z-score}|_{\text{SI expression}} \leq 1$. For regulated intron-containing transcripts that do not belong to one of these categories, we considered we could not confidently determine their type of regulation.

Data availability

The data discussed in this publication have been deposited in NCBI's Gene Expression Omnibus (Edgar *et al*, 2002) and are accessible through GEO Series accession number GSE210071 (http://www.ncbi.nlm.nih.gov/geo/query/acc.cgi?acc=GSE210071).

Expanded View for this article is available online.

Acknowledgements

We thank members of the Scheiffele lab for advice and constructive discussions. We thank Eric Allemand, Özgür Genç, Raul Ortiz and Madalena Pinto for constructive discussions and comments on the manuscript. We are grateful to Caroline Bornmann, Laetitia Burklé and Sabrina Innocenti for technical support. We thank the Biozentrum Proteomics Core Facility, in particular Alexander Schmidt, for conducting proteomics analysis, the Biozentrum Imaging Core Facility and the Quantitative Genomics Facility of Basel, in particular Philippe Demougin and Christian Beisel. We also thank Pierre De La Grange and Noémie Robil from Genosplice for support in data analysis. O.M. was financed with an Ambizione grant evaluated by the Swiss National Science Foundation (PZ00P3_174153) and with a Novartis Universität Basel Excellence

Scholarships for Life Sciences (3BZ21O2). This work was supported by funds to O.M. from the Swiss National Science Foundation (PZ00P3_174153) and to P.S. from a European Research Council Advanced Grant (SPLICECODE). Open access funding provided by Universitat Basel. Open access funding provided by Universitat Basel.

Author contributions

Maxime Mazille: Data curation; formal analysis; investigation; visualization; writing – original draft; writing – review and editing. **Katarzyna Buczak:** Data curation; formal analysis; writing – review and editing. **Peter Scheiffele:** Conceptualization; resources; supervision; funding acquisition; validation; writing – original draft; writing – review and editing. **Oriane Mauger:** Conceptualization; resources; data curation; formal analysis; supervision; funding acquisition; validation; investigation; visualization; writing – original draft; writing – review and editing.

In addition to the CRediT author contributions listed above, the contributions in detail are:

MM and OM conducted the experiments and performed the computational analysis. KB conducted the mass spectrometry assays. OM, MM and PS designed the experiments and wrote the paper.

Disclosure and competing interests statement

The authors declare that they have no conflict of interest.

References

Bahar Halpern K, Caspi I, Lemze D, Levy M, Landen S, Elinav E, Ulitsky I, Itzkovitz S (2015) Nuclear retention of mRNA in mammalian tissues. *Cell Rep* 13: 2653 – 2662

Battich N, Stoeger T, Pelkmans L (2015) Control of transcript variability in single mammalian cells. *Cell* 163: 1596 – 1610

Bergkessel M, Whitworth GB, Guthrie C (2011) Diverse environmental stresses elicit distinct responses at the level of pre-mRNA processing in yeast. *RNA* 17: 1461 – 1478

Boutz PL, Bhutkar A, Sharp PA (2015) Detained introns are a novel, widespread class of post-transcriptionally spliced introns. *Genes Dev* 29: 63 – 80

Braunschweig U, Barbosa-Morais NL, Pan Q, Nachman EN, Alipanahi B, Gonatopoulos-Pournatzis T, Frey B, Irimia M, Blencowe BJ (2014) Widespread intron retention in mammals functionally tunes transcriptomes. *Genome Res* 24: 1774 – 1786

Brockmann MM, Maglione M, Willmes CG, Stumpf A, Bouazza BA, Velasquez LM, Grauel MK, Beed P, Lehmann M, Gimber N *et al* (2019) RIM-BP2 primes synaptic vesicles via recruitment of Munc13-1 at hippocampal mossy fiber synapses. *eLife* 8: 1 – 22

Cagnetta R, Frese CK, Shigeoka T, Krijgsveld J, Holt CE (2018) Rapid Cue-specific remodeling of the nascent axonal proteome. *Neuron* 99: 29 – 46

Chang DD, Sharp PA (1989) Regulation by HIV rev depends upon recognition of splice sites. *Cell* 59: 789 – 795

Chen X, Rahman R, Guo F, Rosbash M (2016) Genome-wide identification of neuronal activity-regulated genes in *Drosophila*. *eLife* 5: 1 – 21

Darzacq X, Shav-Tal Y, de Turris V, Brody Y, Shenoy SM, Phair RD, Singer RH (2007) *In vivo* dynamics of RNA polymerase II transcription. *Nat Struct Mol Biol* 14: 796 – 806

Dobin A, Davis CA, Schlesinger F, Drenkow J, Zaleski C, Jha S, Batut P, Chaisson M, Gingeras TR (2013) STAR: Ultrafast universal RNA-seq aligner. *Bioinformatics* 29: 15 – 21

Edgar R, Domrachev M, Lash AE (2002) Gene expression omnibus: NCBI gene expression and hybridization array data repository. *Nucleic Acids Res* 30: 207 – 210

Fuchs G, Voichek Y, Benjamin S, Shlomit G, Ido A, Oren M (2014) 4sUDRB-seq: measuring genomewide transcriptional elongation rates and initiation frequencies within cells. *Genome Biol* 15: R69

Gill J, Park Y, McGinnis JP, Perez-Sanchez C, Blanchette M, Si K (2017) Regulated intron removal integrates motivational state and experience. *Cell* 169: 836 – 848

Gottmann K, Mittmann T, Lessmann V (2009) BDNF signaling in the formation, maturation and plasticity of glutamatergic and GABAergic synapses. *Exp Brain Res* 199: 203 – 234

Grabski DF, Broseus L, Kumari B, Rekosh D, Hammarskjold ML, Ritchie W (2021) Intron retention and its impact on gene expression and protein diversity: a review and a practical guide. *Wiley Interdiscip Rev RNA* 12: e1631

de la Grange P, Dutertre M, Martin N, Auboeuf D (2005) FAST DB: a website resource for the study of the expression regulation of human gene products. *Nucleic Acids Res* 33: 4276 – 4284

Green ID, Pinello N, Song R, Lee Q, Halstead JM, Kwok C-T, Wong ACH, Nair SS, Clark SJ, Roediger B *et al* (2020) Macrophage development and activation involve coordinated intron retention in key inflammatory regulators. *Nucleic Acids Res* 48: 6513 – 6529

Greer PL, Greenberg ME (2008) From synapse to nucleus: Calcium-dependent gene transcription in the control of synapse development and function. *Neuron* 59: 846 – 860

Haltenhof T, Kotte A, De Bortoli F, Schiefer S, Meinke S, Emmerichs AK, Petermann KK, Timmermann B, Imhof P, Franz A *et al* (2020) A conserved kinase-based body-temperature sensor globally controls alternative splicing and gene expression. *Mol Cell* 78: 57 – 69

Harward SC, Hedrick NG, Hall CE, Parra-Bueno P, Milner TA, Pan E, Laviv T, Hempstead BL, Yasuda R, McNamara JO (2016) Autocrine BDNF-TrkB signalling within a single dendritic spine. *Nature* 538: 99 – 103

Jacob AG, Smith CWJ (2017) Intron retention as a component of regulated gene expression programs. *Hum Genet* 136: 1043 – 1057

Kilchert C, Wittmann S, Passoni M, Shah S, Granneman S, Vasiljeva L (2015) Regulation of mRNA levels by decay-promoting introns that recruit the exosome specificity factor Mmi1. *Cell Rep* 13: 2504 – 2515

Lackinger M, Sungur AÖ, Daswani R, Soutschek M, Bicker S, Stemmler L, Wüst T, Fiore R, Dieterich C, Schwarting RK *et al* (2019) A placental mammal-specific micro RNA cluster acts as a natural brake for sociability in mice. *EMBO Rep* 20: e46429

Lambert WM, Xu C-F, Neubert TA, Chao MV, Garabedian MJ, Jeanneteau FD (2013) Brain-derived neurotrophic factor signaling rewrites the glucocorticoid transcriptome via glucocorticoid receptor phosphorylation. *Mol Cell Biol* 33: 3700 – 3714

Legrain P, Rosbash M (1989) Some cis- and trans-acting mutants for splicing target pre-mRNA to the cytoplasm. *Cell* 57: 573 – 583

Liu KSY, Siebert M, Mertel S, Knoche E, Wegener S, Wichmann C, Matkovic T, Muhammad K, Depner H, Mettke C *et al* (2011) RIM-binding protein, a central part. *Science* 334: 1565 – 1569

Mardinly AR, Spiegel I, Patrizi A, Centofante E, Bazinet JE, Tzeng CP, Mandel-Brehm C, Harmin DA, Adesnik H, Fagiolini M *et al* (2016) Sensory experience regulates cortical inhibition by inducing IGF1 in VIP neurons. *Nature* 531: 371 – 375

Marquez Y, Höpfler M, Ayatollahi Z, Barta A, Kalyna M (2015) Unmasking alternative splicing inside protein-coding exons defines exitrons and their role in proteome plasticity. *Genome Res* 25: 995 – 1007

Marty V, Labialle S, Bortolin-Cavaillé ML, De Medeiros GF, Moisan MP, Florian C, Cavaillé J (2016) Deletion of the miR-379/miR-410 gene cluster at the imprinted Dlk1-Dio3 locus enhances anxiety-related behaviour. *Hum Mol Genet* 25: 728 – 739

Matter N, Herrlich P, König H (2002) Signal-dependent regulation of splicing via phosphorylation of Sam68. *Nature* 420: 691 – 695

Mauger O, Lemoine F, Scheiffele P (2016) Targeted intron retention and excision for rapid gene regulation in response to neuronal activity. *Neuron* 92: 1266 – 1278

Naro C, Jolly A, Di Persio S, Bielli P, Setterblad N, Alberdi AJ, Vicini E, Geremia R, De la Grange P, Sette C (2017) An orchestrated intron retention program in meiosis controls timely usage of transcripts during germ cell differentiation. *Dev Cell* 41: 82 – 93

Ninomiya K, Kataoka N, Hagiwara M (2011) Stress-responsive maturation of Clk1/4 pre-mRNAs promotes phosphorylation of SR splicing factor. *J Cell Biol* 195: 27 – 40

Ortíz R, Georgieva MV, Gutierrez S, Pedraza N, Fernández- SM, Gallego C (2017) Recruitment of Staufen2 enhances dendritic localization of an intron- containing CaMKIIα mRNA. *Cell Rep* 20: 13 – 20

Park SK, Zhou X, Pendleton KE, Hunter OV, Kohler JJ, O'Donnell KA, Conrad NK (2017) A conserved splicing silencer dynamically regulates O-GlcNAc transferase intron retention and O-GlcNAc homeostasis. *Cell Rep* 20: 1088 – 1099

Parra M, Booth BW, Weiszmann R, Yee B, Yeo GW, Brown JB, Celniker SE, Conboy JG (2018) An important class of intron retention events in human erythroblasts is regulated by cryptic exons proposed to function as splicing decoys. *RNA* 24: 1255 – 1265

Pendleton KE, Chen B, Liu K, Hunter OV, Xie Y, Tu BP, Conrad NK (2017) The U6 snRNA m 6 a methyltransferase METTL16 regulates SAM synthetase intron retention. *Cell* 169: 824 – 835

Pendleton KE, Park SK, Hunter OV, Bresson SM, Conrad NK (2018) Balance between MAT2A intron detention and splicing is determined cotranscriptionally. *RNA* 24: 778 – 786

Pimentel H, Parra M, Gee SL, Mohandas N, Pachter L, Conboy JG (2016) A dynamic intron retention program enriched in RNA processing genes regulates gene expression during terminal erythropoiesis. *Nucleic Acids Res* 44: 838 – 851

Prasanth KV, Prasanth SG, Xuan Z, Hearn S, Freier SM, Bennett CF, Zhang MQ, Spector DL (2005) Regulating gene expression through RNA nuclear retention. *Cell* 123: 249 – 263

Quesnel-Vallières M, Dargaei Z, Irimia M, Gonatopoulos-Pournatzis T, Ip JY, Wu M, Sterne-Weiler T, Nakagawa S, Woodin MA, Blencowe BJ *et al* (2016) Misregulation of an activity-dependent splicing network as a common mechanism underlying autism Spectrum disorders. *Mol Cell* 64: 1023 – 1034

Russek SJ, Hixson KM, Cogswell M, Brooks-Kayal AR, Russek SJ (2019) Transcriptomic analysis of the BDNF-induced JAK / STAT pathway in neurons: a window into epilepsy-associated gene expression. *bioRxiv* https://doi.org/10.1101/577627 [PREPRINT]

Schindelin J, Arganda-Carreras I, Frise E, Kaynig V, Longair M, Pietzsch T, Preibisch S, Rueden C, Saalfeld S, Schmid B *et al* (2012) Fiji: An open-source platform for biological-image analysis. *Nat Methods* 9: 676 – 682

Sharangdhar T, Sugimoto Y, Heraud-Farlow J, Fernández-Moya SM, Ehses J, Ruiz de los Mozos I, Ule J, Kiebler MA (2017) A retained intron in the 3′-UTR of Calm3 mRNA mediates its Staufen2- and activity-dependent localization to neuronal dendrites. *EMBO Rep* 18: 1762 – 1774

Shin C, Manley JL (2004) Cell signalling and the control of pre-mRNA splicing. *Nat Rev Mol Cell Biol* 5: 727 – 738

Sibley CR, Emmett W, Blazquez L, Faro A, Haberman N, Briese M, Trabzuni D, Ryten M, Weale ME, Hardy J *et al* (2015) Recursive splicing in long vertebrate genes. *Nature* 521: 371 – 375

Singh J, Padgett RA (2009) Rates of *in situ* transcription and splicing in large human genes. *Nat Struct Mol Biol* 16: 1128 – 1133

Spiegel I, Mardinly AR, Gabel HW, Bazinet JE, Couch CH, Tzeng CP, Harmin DA, Greenberg ME (2014) Npas4 regulates excitatory-inhibitory balance within neural circuits through cell-type-specific gene programs. *Cell* 157: 1216 – 1229

Suzuki K, Bose P, Leong-Quong RY, Fujita DJ, Riabowol K (2010) REAP: a two minute cell fractionation method. *BMC Res Notes* 3: 294

Tennyson C, Klamut H, Worton R (1995) The human dystrophin gene requires 16 hours to be transcribed and is cotranscriptionally spliced. *Nat Genet* 9: 184 – 190

Tyssowski KM, Gray JM (2019) The neuronal stimulation–transcription coupling map. *Curr Opin Neurobiol* 59: 87 – 94

Ullrich S, Guigó R (2020) Dynamic changes in intron retention are tightly associated with regulation of splicing factors and proliferative activity during B-cell development. *Nucleic Acids Res* 48: 1327 – 1340

Veloso A, Kirkconnell KS, Magnuson B, Biewen B, Paulsen MT, Wilson TE, Ljungman M (2014) Rate of elongation by RNA polymerase II is associated with specific gene features and epigenetic modifications. *Genome Res* 24: 896 – 905

Wiśniewski JR, Gaugaz FZ (2015) Fast and sensitive total protein and peptide assays for proteomic analysis. *Anal Chem* 87: 4110 – 4116

Wong JJ-L, Ritchie W, Ebner OA, Selbach M, Wong JWH, Huang Y, Gao D, Pinello N, Gonzalez M, Baidya K *et al* (2013) Orchestrated intron retention regulates normal granulocyte differentiation. *Cell* 154: 583 – 595

Yang X, Coulombe-Huntington J, Kang S, Sheynkman GM, Hao T, Richardson A, Sun S, Yang F, Shen YA, Murray RR *et al* (2016) Widespread expansion of protein interaction capabilities by alternative splicing. *Cell* 164: 805 – 817

Yap K, Lim ZQ, Khandelia P, Friedman B, Makeyev EV (2012) Coordinated regulation of neuronal mRNA steady-state levels through developmentally controlled intron retention. *Genes Dev* 26: 1209 – 1223

Yeo G, Burge C (2004) Maximum entropy modeling of short sequence motifs with applications to RNA splicing signals. *J Comput Biol* 11: 377 – 394

Yeom K-H, Pan Z, Lin C-H, Lim HY, Xiao W, Xing Y, Black DL (2021) Tracking pre-mRNA maturation across subcellular compartments identifies developmental gene regulation through intron retention and nuclear anchoring. *Genome Res*: 1106 – 1119

Zhou Z, Qiu J, Liu W, Zhou Y, Plocinik RM, Li H, Hu Q, Ghosh G, Adams JA, Rosenfeld MG *et al* (2012) The Akt-SRPK-SR Axis constitutes a major pathway in transducing EGF signaling to regulate alternative splicing in the nucleus. *Mol Cell* 47: 422 – 433